ELECTROSTATIC CONFINEMENT OF AN ALKALI METAL PLASMA

by

MORRY JAFFE

A dissertation submitted to the Graduate Faculty in Physics in partial fullfillment of the requirements for the degree of Doctor of Philosophy, The City University of New York.

1971

This manuscript has been read and accepted for the Graduate Faculty in Physics in satisfaction of the dissertation requirement for the degree of Doctor of Philosophy

6/25/71
date

Chairman of Examining Committee

6/25/71
date

Executive Officer

Supervisory Committee

The City University of New York

ACKNOWLEDGMENTS

My thanks and gratitude go first of all to Professor Joseph C. Cataldo, the director and prime mover of this project. His leadership, financial and moral assistance has made this effort succeed. My thanks also go to Professor Norman C. Jen for stimulating conversations, for making the CCNY Magnetohydrodynamics Laboratory available to me and for arranging additional financial and other support for myself.

I wish to acknowledge the vital assistance of Professors A.M. Levine and K.C. Rogers in providing advice and acquainting me with some necessary theory for this dissertation, as well as Professor M. Mittleman for assistance in literature research.

In addition to the above members of my Guidance Committee, I wish to thank Professors C.M. Tchen and T.H. Stix for useful discussion of some theoretical aspects of this work, as well as Professor M. Ettenberg for making his personal library available to me.

Thanks go to Mr. Ira Mansfield, our colleague in the MHD Lab for his expert assistance in data gathering and maintenance. I am indebted to Dr. C. Tao for use of the radial particle collector

that he built and calibrated, to Mr. Fred Benkovsky of the Civil Engineering Shop for construction of some of the experimental apparatus, and to Mr. Mitch Haspel for the use of his impregnated cathode emitter. Many thanks go to Messrs Jerry Cannella, Jack Giampetro, Mike Kolba, Joe Lane, Pat Lynch and Al Venditti of the Physics Shop.

Finally, I gratefully acknowledge the Physics Department for carrying me on through this struggle, the Civil Engineering Department for letting a "foreigner" use its services, and the Air Force Office of Scientific Research (Grant No.1093-69) and National Science Foundation (Grant No. GK 5230) as the source of my financial support.

TABLE OF CONTENTS

LIST OF FIGURES

Abstract

ELECTROSTATIC CONFINEMENT

OF AN ALKALI METAL PLASMA

A series of experiments have been performed related to electrostatic confinement of a plasma within a radial potential well generated in part by a 1-2 keV peripheral beam of electrons in a low β potassium plasma.

The imposition of a beam of electrons about a Q-machine plasma column serves to deepen the radial potential well across that column. The transverse plasma flux is consequently decreased, and the peak ion density and endplate collector current rise an order of magnitude. The same holds true for injection of a thin envelope of 1-2 kV electrons from an impregnated cathode ring emitter. Both radial and terminal particle collectors were used to measure transverse flux.

A theoretical calculation was made of the flux of ions in the plasma column with energy sufficient to surmount the potential well. From this, an expression was derived relating the ratio of I_i/n for one well depth to I_i/n for a different well depth. A comparison was made with suitable empirical data taken with the peripheral beam (deep well) and without the beam (shallow well) surrounding the column. This

comparison was found to be quite good. The deepening of the well by this beam is attributed to its effect upon the end condition.

Plasma cells were studied in this Q-device under a great variety of conditions; their origin was found to be due to a circular beam of electrons from the periphery of the bombarding filament moving around the tungsten cathode and entering the column with considerable transverse as well as longitudinal velocity. The cells per se were not found to improve confinement.

CHAPTER I

INTRODUCTION

Until quite recently, research aimed toward improving plasma confinement has concentrated almost exclusively on magnetic field geometries and schemes. Proposals have been made for devices that rely on a radial electrostatic field as the major confining force. Such fields have been considered in large toroidal devices but only in terms of maintaining equilibrium, not as the confining mechanism. A combination of magnetic and electric forces may well be free from the many types of instability encountered with pure magnetic confinement.

In this work a series of experiments have been done in which radial electric fields have been created by a fast electron beam in a Q-machine, the depth of the resulting potential well measured and correlated with measured transverse plasma flux. Comparison with the calculated effect of the well has been made.

Plasma cells that have been previously reported for this Q-machine have been further studied and their origin determined.

Part A - Review of Plasma Diffusion

The subject of diffusion of a magnetoplasma in the

direction perpendicular to the field over and above that due to collisional random walk has been under investigation subsequent to Bohm's initial experimental and theoretical study of the subject in a gaseous discharge[1]. Whereas in simple collisional (classical) diffusion, the transverse diffusion coefficient $D_\perp$ varies as B^{-2}, the so-called anomalous or Bohm diffusion coefficient varies as B^{-1} and is, in general, several orders of magnitude greater than the former. Bohm attributed this to "hash" or turbulent electric fields of high amplitude in the discharge. No complete calculation has been made of turbulent diffusion[2].

Early attempts to measure or estimate transverse diffusion in a Q-machine were inconclusive, some investigators finding classical type diffusion, others finding Bohm-type diffusion, some finding neither, depending on various conditions such as plasma density and range of magnetic field[3-6]. Most study of anomalous transverse diffusion in a Q-machine has dealt with the non-turbulent type; that due to radial drift.

One source of this drift is time-varying, but non-random, electric field in the $\hat{\theta}$ direction (giving rise to E_θ x Bz drift in the $\hat{r}$ direction) due to plasma oscillation excited by various "universal" instabilities. Buchelnikova and coworkers measured $D_\perp$ and correlate its magnitude with the amplitude of the observed oscillation[7-10]. $D_\perp$ was found to be invariant of B for plasma densities in the 10^9 -10^{10} cm^{-3} range. Chen has studied and calculated transverse

plasma flux due to resistive overstability[11]. Chu, Hendel and Politzer find enhanced plasma loss in a Q-machine due to collisional drift instability, but not according to the Bohm formula[12,13]. Wolf and Rogers measured $D_\perp$, finding classical type diffusion in an undisturbed plasma column and anomalous diffusion when an energetic low density ($\sim 10^6$ cm^{-3}) electron beam excited plasma waves[14,15]. Eastlund and coworkers measured $D_\perp$ in a pulsed plasma Q-machine and find positive dependence on frequency and amplitude of externally and self-excited plasma waves[16-18].

The other source of radial drift studied in Q-machines is that due to azimuthal temperature gradient in the column caused by a similar gradient on the hot plate surface. Such an effect has been investigated by Chen[19]. Decker et al measured $D_\perp$ in a Q-machine and found quantitative explanation for $D_\perp$ in terms of ∇TXB drift[20]. They report no correlation of $D_\perp$ with plasma oscillation in any way.

Subsequent to identification of these losses, work proceeded upon schemes for suppressing the cause of these losses. Simonen, Chu, and Hendel stabilized their Q-machine plasma by feedback and reported a drop in transverse diffusion[21]. Jassby and Motley constructed a hot plate designed to greatly reduce azimuthal temperature variation and reported improved confinement with its use[22]. Guilino nearly eliminated azimuthal temperature variation by rotating the hot plates in his double-ended device; a claimed ten to sixty-fold reduction in $D_\perp$ was achieved[23]. Chen and

coworkers attacked both sources of radial drift by imposing magnetic shear on their plasma column, resulting in twisting the plasma equipotentials in a spiral pattern[24-27]. This symmetrizes the column; a sizeable drop in transverse diffusion was reported.

Until quite recently devices and schemes for plasma confinement by a field have dealt exclusively with magnetic field geometries. A toroidal device for stripping and accelerating ions has been constructed, using an electron cloud to create a deep radial potential well to confine the ions[28,29]. Diffusion in such a device has not been studied.

Part B - Review of Electron Beam - Plasma Interaction

Most work dealing with electron beam-plasma interaction has centered on production of a sparse plasma in a neutral gas by the beam. Much study has taken place in recent years of the creation of plasma waves of many types and frequency ranges by an electron beam[30-40]. Among these is a transfer of the diocotron or slipping stream instability of an electron beam to a plasma for which the ion cyclotron frequency is near that of the diocotron instability[41]. In a Q-machine, electron beams have been used to excite plasma waves. Several investigators have reported heating of plasma electrons as a result, and increase in transverse ionic

temperature. Eastlund et al[16-18] reported a consequent increase in $D_\perp$ as did Wolf and Rogers[15]. Astrelin et al attribute increase in convective diffusion due to this transverse ionic heating[42].

Field et al investigated the confining effect on an electron beam in vacuo of an ionic pencil created in its path[43]. Gizton and Wadia have created an electrostatic trap for these ions to maintain this effect[44]. Hines et al studied this effect in a magnetic field[45].

Creation of a very intense electron beam of relativistic energy has been proposed for the creation of a magnetic bottle (E layer) for confinement of a thermonuclear plasma[46].

Another device has been proposed (and a forerunner built) to strip and confine heavy ions by immersing them in a relatively dense cloud of fast electrons, which in turn, are confined by a toroidal magnetic field[28, 29]. A radial potential well of 20 million volt depth is envisioned for this device (HIPAC).

Part C - Plasma Cells and Electron Beam Breakup

The term plasma cell has loosely been applied to any type of vortex or closed circulation of plasma in a volume smaller than the volume of the entire body of the plasma. Ring vortices of metallic and deuterium ions have been created and projected by a plasma gun and studied by Bostick,

Wells, and others[47-55]. Wells has succeeded in trapping such a vortex for several milliseconds[56]. Closed circulation of plasma around current carrying hoops in an octupole device has been observed by several investigators[57]. Diffusion of plasma in this field geometry was the major subject of study here. Harries and others have reported short-lived ($\sim$ 1msec) convective cells in an rf heated hydrogen-helium plasma in a linear quadrupole device, suggesting that this convection contributes to plasma loss[58-60]. Barney and Sprott have studied double vortex flows in toroidal octupole and linear quadrupole devices, with particular attention to their trajectories[61]. Chen, Mosher, and Rogers, investigating an alkali metal plasma in a Q-machine with an axial current-carrying rod through its center, have inferred the existence of spiral convective cells through a twisted set of equipotentials with their sheared field geometry[62]. A stationary cell-like pattern has been photographed and studied by Cataldo; the cells being attributed to a stationary convective instability, much akin to hydrodynamic Taylor cells[63,64].

Basic research into vacuum tube microwave devices has led to the discovery of breakup of a tubular beam of electrons travelling parallel to a uniform magnetic field. Kyhl and Webster[65-67], and Cutler[68] have photographed a pattern of "vortex-like current bundles" or "spiral nebula" resulting from this breakup. Theoretical analysis is given by Kyhl and Webster[65], and Pierce[69] based on the linearized

equation of motion and normal mode analysis, reporting agreement with experimental data.

Part D - Summary and Outline of Chapters II - V

This chapter serves to introduce the proposed experimental investigation and calculation of improved plasma confinement in a Q-machine by electrostatic means. Reviews of the subjects of electron beam-plasma interaction, diffusion in a Q-machine and attempts to reduce it, and cells in plasma devices have been presented.

Four chapters remain; chapter II deals with the experimental apparatus used in this work, Q-machine and associated diagnostics. The experimental procedure and results are presented in chapter III with particular emphasis on the association of radial potential well depth and transverse plasma flux. Chapter IV includes calculation of the confining efficacy of the potential well, estimation of the deepening of this well, and investigation of oscillation in an electron beam, calculation of ionization by the beam and electron trajectory calculation related to cellular genesis. A summary of the major features of the experiments, comparison of these with theoretical calculation and conclusions based on the latter comprise chapter V.

CHAPTER II

DESCRIPTION OF EXPERIMENTAL APPARATUS

The plasma experiments herein described have been performed within the Q-machine at the City College magneto-hydrodynamics laboratory[70]. The Q-machine is a device for creating and analysing a quiescent highly-ionized alkali-metal columnar magnetoplasma[71].

Some significant alterations of the plasma generator have been made for some of these experiments. Transverse diffusion is independently measured using radial[7,8] and terminal particle collectors[20,72]. The Q-machine is operated in both single[20] and double-ended modes[71]. One and two dimensional Langmuir probes are employed[73]. The plasma camera[74-76], used with single-ended operation, affords a visual profile of the plasma column.

Part A - Q-Machine

1) Chamber

The City College Q-machine[70], Fig. 2-1, is basically a cylindrical stainless steel chamber open at both ends, 4-3/4 inches inner diameter, 54 inches long. A water jacket with alternate flow system provides chamber wall cooling at constant temperature throughout the inner

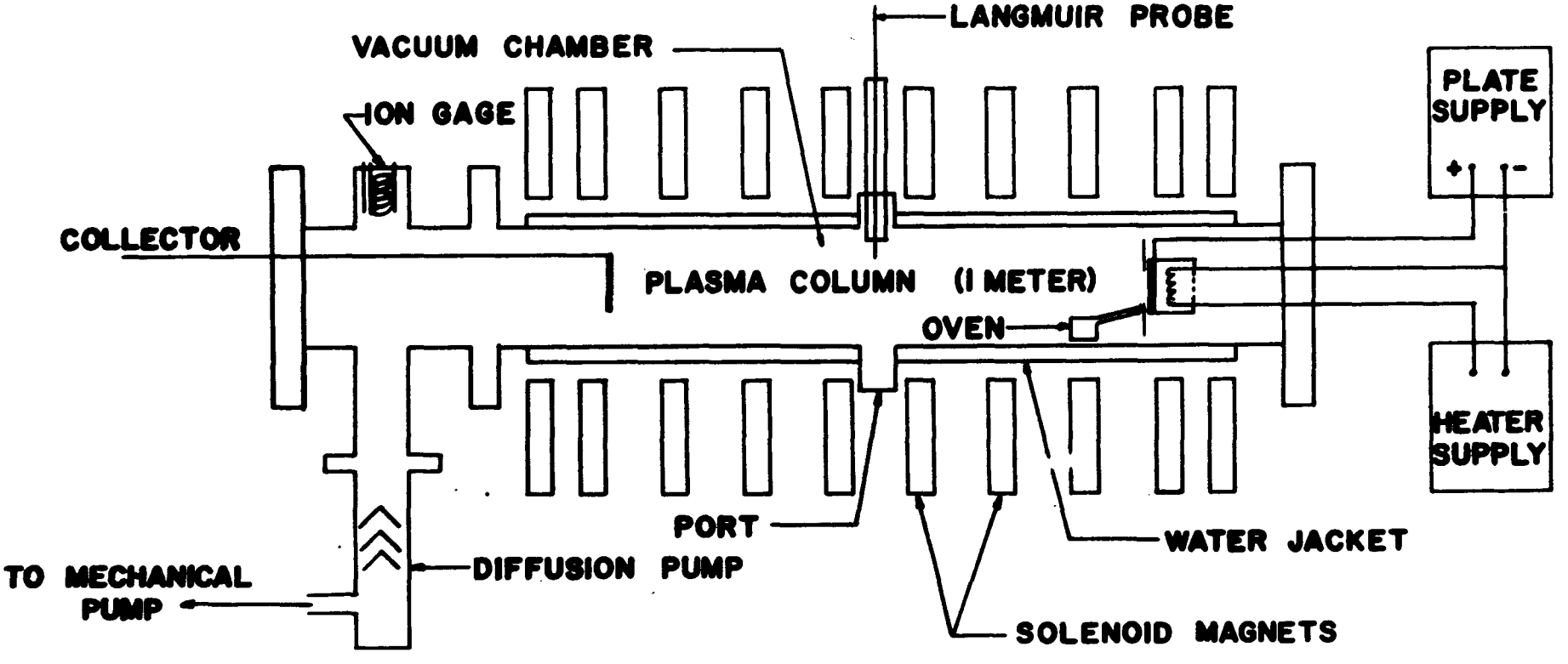

Fig. 2-1 Schematic of Q-machine

surfaces. Neutral atoms and stray ions are thereby condensed on the walls to minimize background. Flanges are provided at both ends for insertion and removal of electrode assembly(ies) or diagnostic devices such as the plasma camera and the terminal particle collector. Other ports provide for high vacuum pumpout, vacuum gauges, and for diagnostic devices. Three 1 inch diameter ports are located at the center of the machine. A 4 inch diameter Consolidated Vacuum Company 750 liters/second diffusion pump, backed by model 1376 Welch Duoseal rotary pump, (10 cu. ft./min) is used to obtain a vacuum within the chamber on the order of 10^{-5} torr. The Bayard-Alpert vacuum gauge is manufactured by Vactronics Inc., and the thermocouple gauge and control panel by Veeco.

2) Magnet

The chamber is girt by 10 water cooled non-ferrous coils, manufactured by Magnion Inc., spaced along the chamber so as to provide a uniform magnetic field within a 4-3/4 inch diameter x 22 inch long experimental volume. A field of up to 10 kG can be created. The associated power supply, manufactured by Richardson-Allen, provides up to 1000 amperes for this purpose.

The variation of the field intensity along the chamber axis is $\pm$ 2.0%, exceeding manufacturer's specifications. The field was measured by moving a Hall probe

radially and axially within the chamber. This gaussmeter has an accuracy of better than 0.1%. As seen in Fig. 2-2, the field is very uniform within a 1 inch diam. central column.

3) Electrode Assemblies

a) Ionizer

The ionizer of the Q-machine is a 1 inch diam. x 1/4 inch thick tungsten disc, electrically grounded, heated by electron bombardment from a tungsten wire filament 5/16 inch behind it biased 1-2 kV below ground. The disc is thereby heated to 2000-2500° K.

The ionization potential of incident potassium atoms is 4.32 volts, lower than the 4.52 volt work function of tungsten. The tungsten disc surface, depleted of electrons by thermionic emission, may therefore accept the loosely bound outer electron from the potassium atoms, leaving them ionized. Several different filament assemblies are employed, not all of which are used only to heat the tungsten disc.

The basic ionization apparatus is illustrated in Fig. 2-3. The circle of pins on which the filament is wound is 0.9375 inch in diameter. The filament plane rests 1/4 inch above the boron nitride holder. A tantalum inner shield, 1 1/2 inches in diameter, extends 9/16 inch above the holder. This shield is at filament potential in order

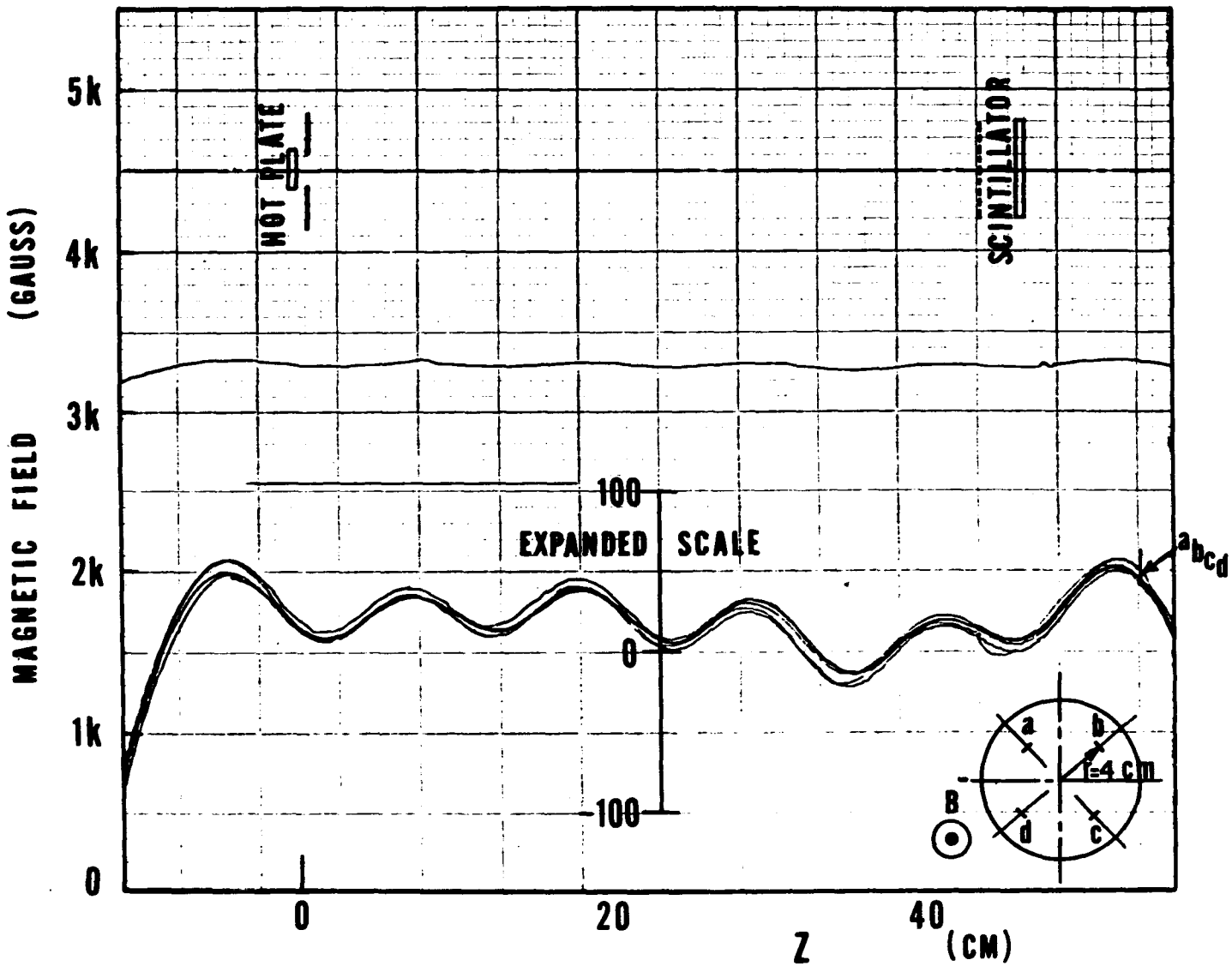

Figure 2-2 Calibration of Magnetic Field Parallel to the Axis of the Test Section

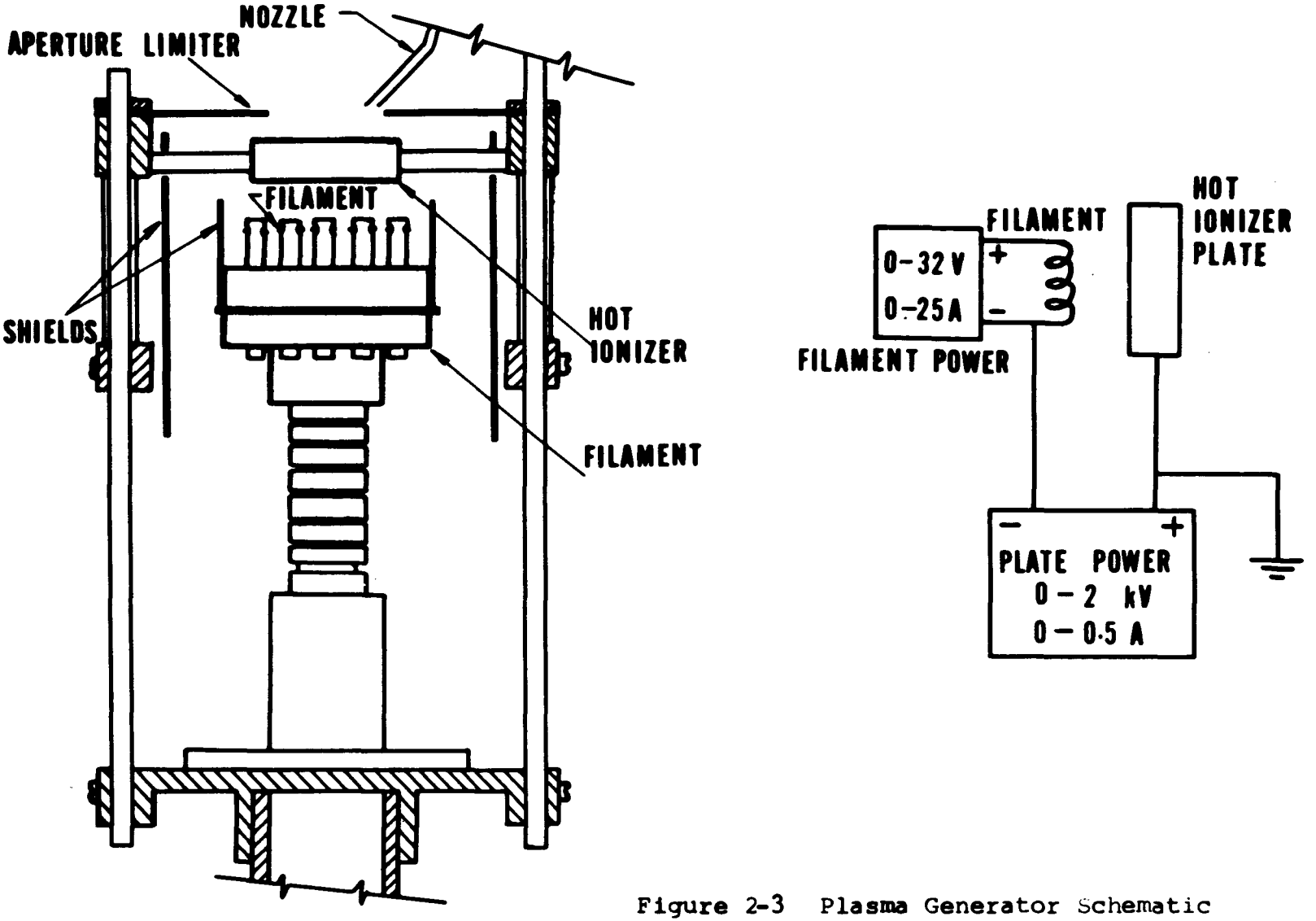

Figure 2-3 Plasma Generator Schematic

to confine the bombarding electrons. Another outer tantalum shield 2 inches in diameter surrounds the ionizer assembly. These shields thermally isolate the hot surfaces to conserve heat. Fig. 2-3 illustrates the circuit.

This diode arrangement operates neither in the space charge limited mode (Langmuir-Childs "3/2 power law") nor in the temperature limited mode. The diode characteristic is illustrated in Fig. 2-4. Deviation from the Langmuir-Childs law is greater at higher pressure, indicating possible ion generation by the beam. Operation is in the space charge limited regime. The temperature of the hot plate varies linearly with plate power. This has been checked with an optical pyrometer (Fig. 2-5). One may then estimate plate temperature from the meters on the power supplies.

In order to produce cells at magnetic fields higher than those at which cells set in with the above arrangement, it was necessary to have an electron emitter placed at a greater distance from the axis than that of the above arrangement. One such configuration consists of wrapping the tungsten wire around the periphery of the holder, isolating it with spacers made of ceramic tubing. Since this puts the outer emitter effectively in series with the diode filament, electron emissions could not be separately controlled. This assembly is used without

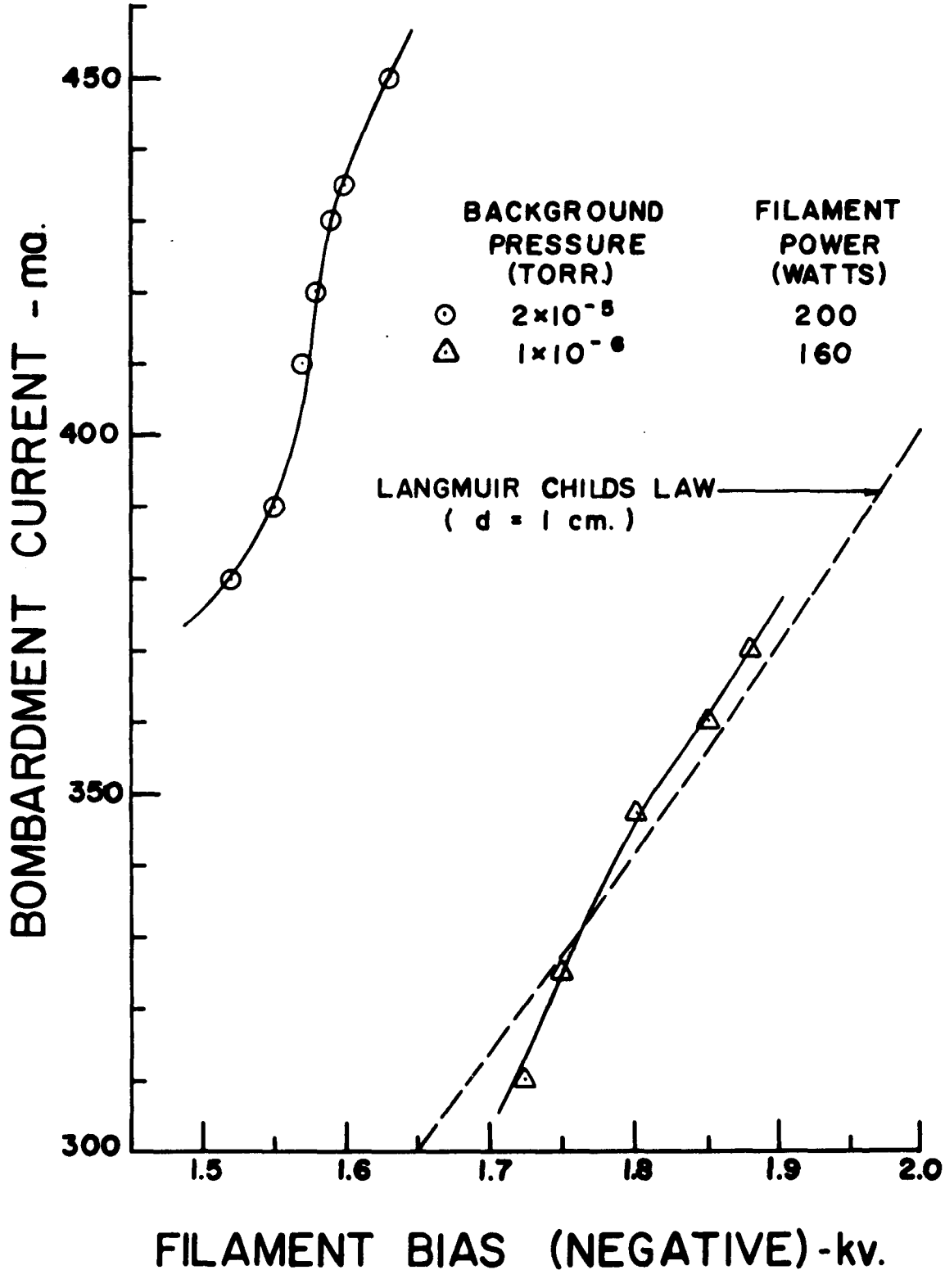

Fig. 2-4 Electron gun characteristics

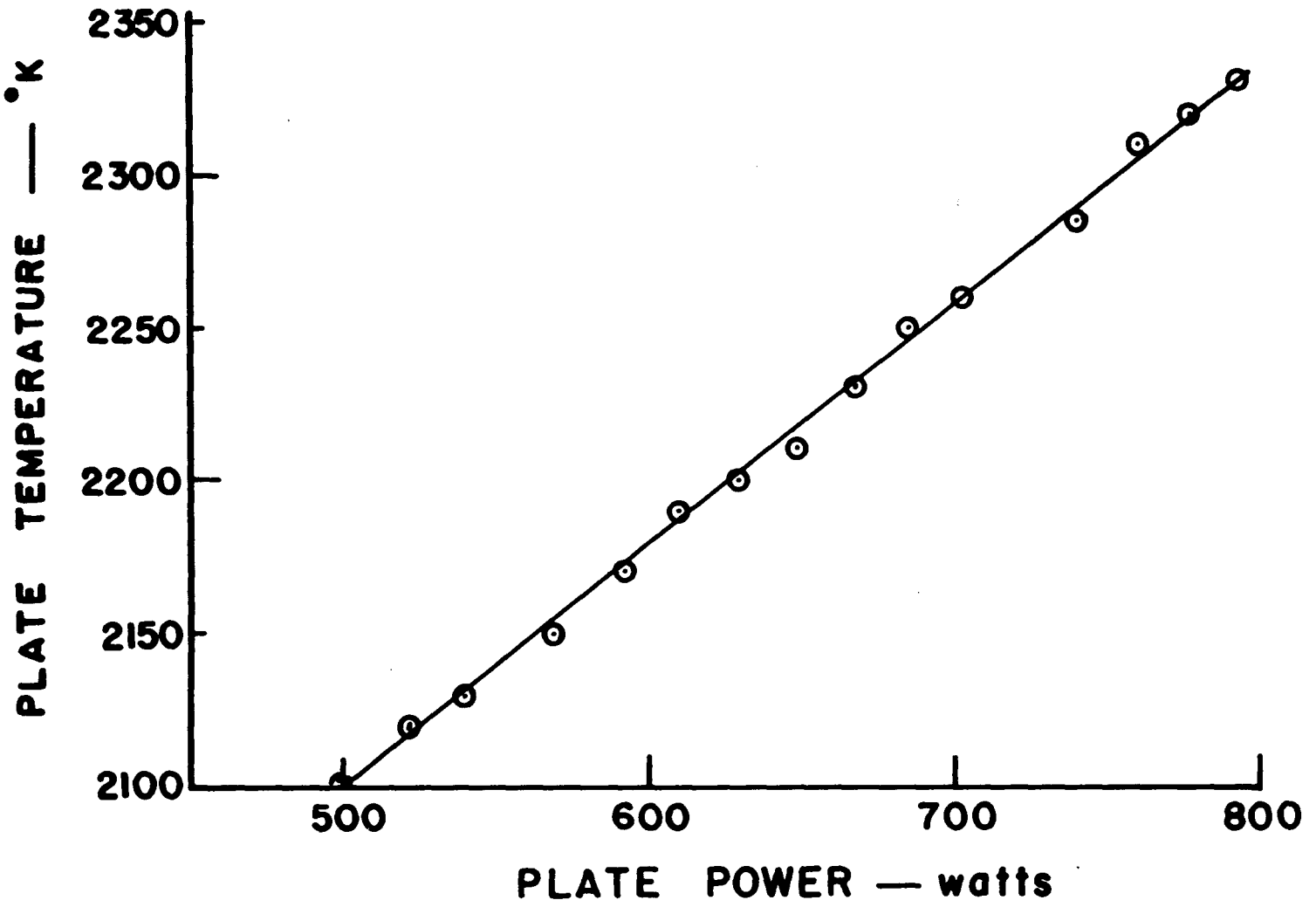

Fig. 2-5 Plate temperature vs plate input power

an inner shield.

In order to effect separate control, an outer filament assembly was constructed and powered by another supply. It consists of a length of .012 inch tungsten wire wrapped around 12 ceramic pins supported by a boron nitride ring. The circle of pins is 1 7/8 inches in diameter. This outer filament is in the same plane as the inner filament. A special stainless steel foil outer shield had to be constructed for this setup.

A Philips Metalonics impregnated cathode electrode gun was also employed to obtain a highly uniform cylindrical electron beam as shown in Fig. 2-6. It is heated by a toroidal coil of 0.020 inch tungsten wire; the torus diameter is 1 inch. The emitting surface is a concave 1 3/16 inch diameter disc with a 13/16 inch hole in the center. The emitter is made of precisely machined porous tungsten, the pores of which are filled with barium calcium aluminates. The toroidal heater sits just below the emitter. A current density capability of 2 1/2 amp/cm at a temperature of 1100^{o} C. is claimed for the emitter. The gun is enclosed in a molybdenum body. Electrical connections are similar to those of the other filament arrangements.

The tungsten hot plate or cathode is supported by three 1/8" diameter tungsten pins from the framework of the electrode assembly. In order to determine whether

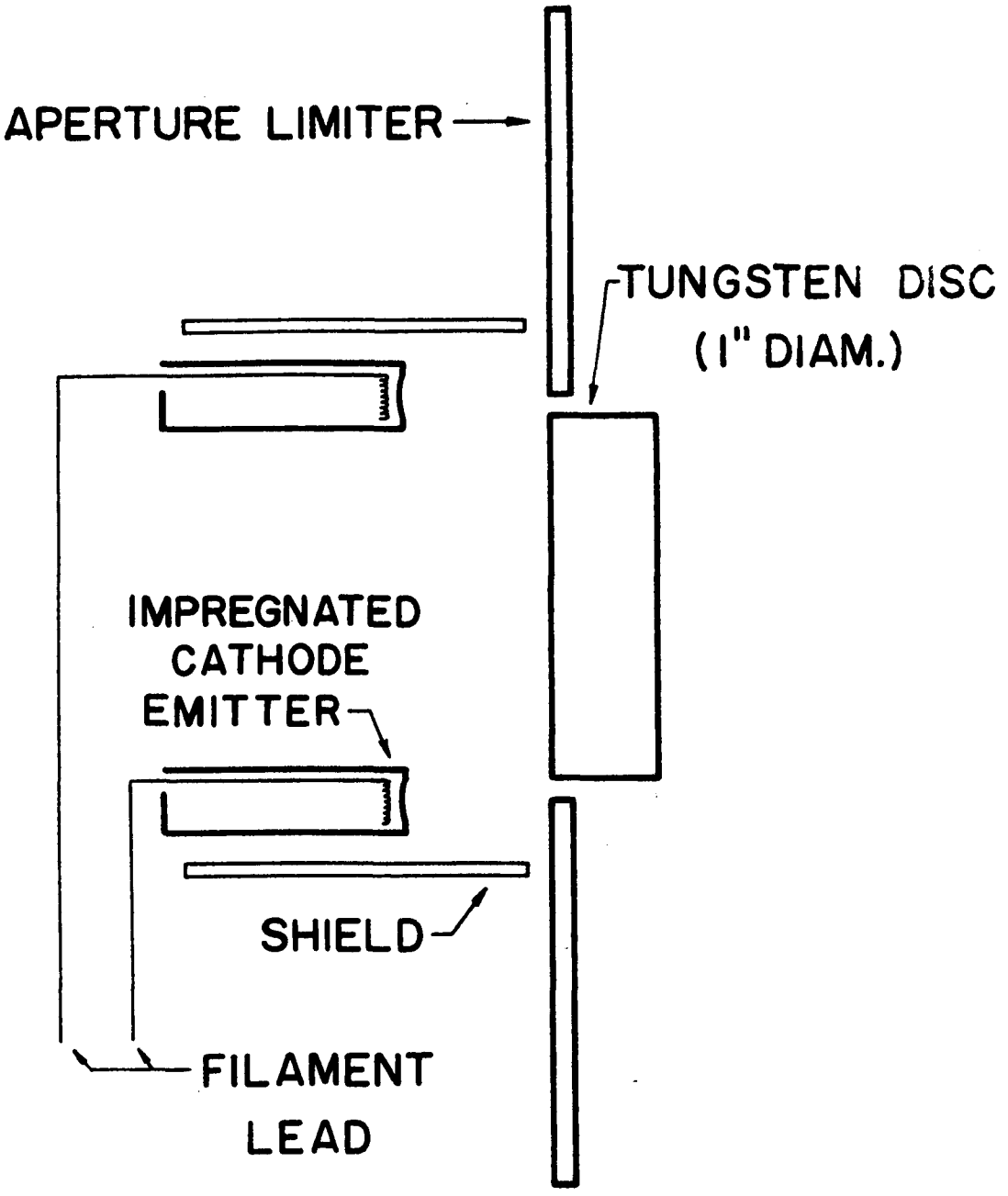

Fig. 2-6 Impregnated Cathode Electrode Gun

the pins were influential in cellular creation, the cathode was replaced by one of a number of stainless steel discs, 1/4 inch in thickness, supported by a screw through a threaded hole in the axis, the screw being supported by a strut downstream. Discs of 1, 7/8, 3/4, 5/8 inch diameter were built. The longitudinal position of the discs was also varied.

A boron nitride electron shield was constructed in order to prevent bombarding electrons from entering the column. It is in the form of a short cylinder, 1/4 inch long, 3/4 inch inner diameter, 1 3/8 inch outer diameter with a 1 inch. i.d. 1/32, inch deep step machined in one end to closely fit the cathode (Fig. 2-7).

In some experiments, a similar filament-hot plate assembly was installed on the side opposite of the Q-machine the electrode assembly for double-ended operation.

The tungsten filaments are powered by dc supplies with 25 amp, 32 volt capacity manufactured by Hazelton of New York City. The diode potentials are established by a pair of 2 kV, 500 ma. dc supplies, along with an external current regulator, also manufactured by Hazelton.

Cathode and other hot surface temperatures are measured with a Leeds and Northrup 8632c optical pyrometer.

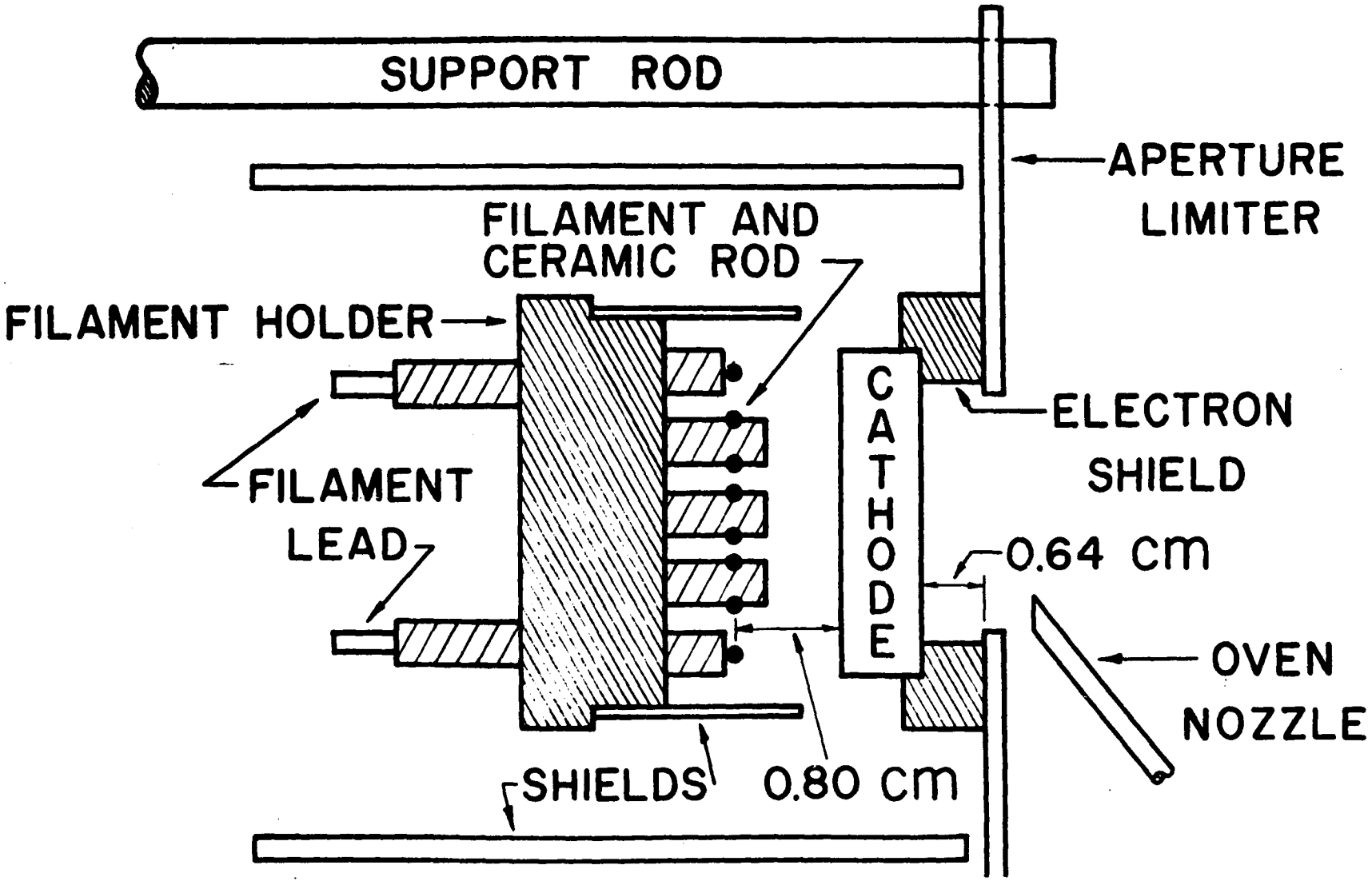

Fig. 2-7 Electrode Assembly with BN Electron Shield Installed

b) Oven

The potassium vapor is supplied from a chamber machined out of a one inch stainless steel cube via a 1/16 inch diameter stainless steel nozzle. The nozzle ends 1/4 inch from the center, 5/16 inch in front of the cathode. A helically wound ceramic jacketed filament of 0.009 inch diameter tungsten wire is inserted through holes in the chamber to heat the latter. Control of temperature is aided by placing a rectangular copper water jacket against one side of the chamber. A copper gasketed plug screws out, enabling the chamber to be filled with metallic potassium from time to time. Electrical connections for the plasma generator and the cooling water supply for the atomic beam oven are made through the stainless steel mounting flange for the plasma generator.

The dc power supply for the oven (28 V, 10 amps capacity) is manufactured by Hazelton. Usually, 2-4 amps. suffice for normal operation.

c) Limiters

So-called aperture limiters (a disc with a hole in it) are used to shape the initial cross-section of the plasma column. An example is illustrated in Fig. 2-7. The limiter is usually placed parallel to and at a distance of 3/16 inch from the cathode. Tantalum

limiters, 0.020 inch thick, with circular central apertures of 1/2, 5/8, 3/4, 7/8, 1, 1-1/16 and 1-3/16 inch diameter were used. A tantalum limiter of similar thickness with a 0.075 inch by 0.675 inch oblong slot was also employed, as well as one with a 3/4 inch diameter circle of sixteen 1/16 inch diameter holes. The tantalum limiters, usually set at ground potential, could be insulated and biased up to $\pm$2 kV. A boron nitride limiter with 3/4 inch central circular aperture was also used.

Part B - Probe

A Langmuir probe is a length of tungsten wire, insulated so as to expose but a short section at the end, inserted into the plasma. Its purpose is to collect current or to determine plasma potential at the probe tip.

The construction of the probes used in these experiments is shown in Fig. 2-8. The probe consists of a 0.008 inch diameter tungsten wire enclosed in a 0.025 inch outer diameter alumina-based ceramic tube. The tube is helically wrapped with 0.001 inch thick o.f.h.c. copper foil to electrostatically shield the probe. The foil is enclosed in a 0.057 inch o.d. ceramic tube. A wire tip exposure of 1 mm is chosen as a compromise between the desireability of large collecting surface to obtain measureable current, and the necessity to localize

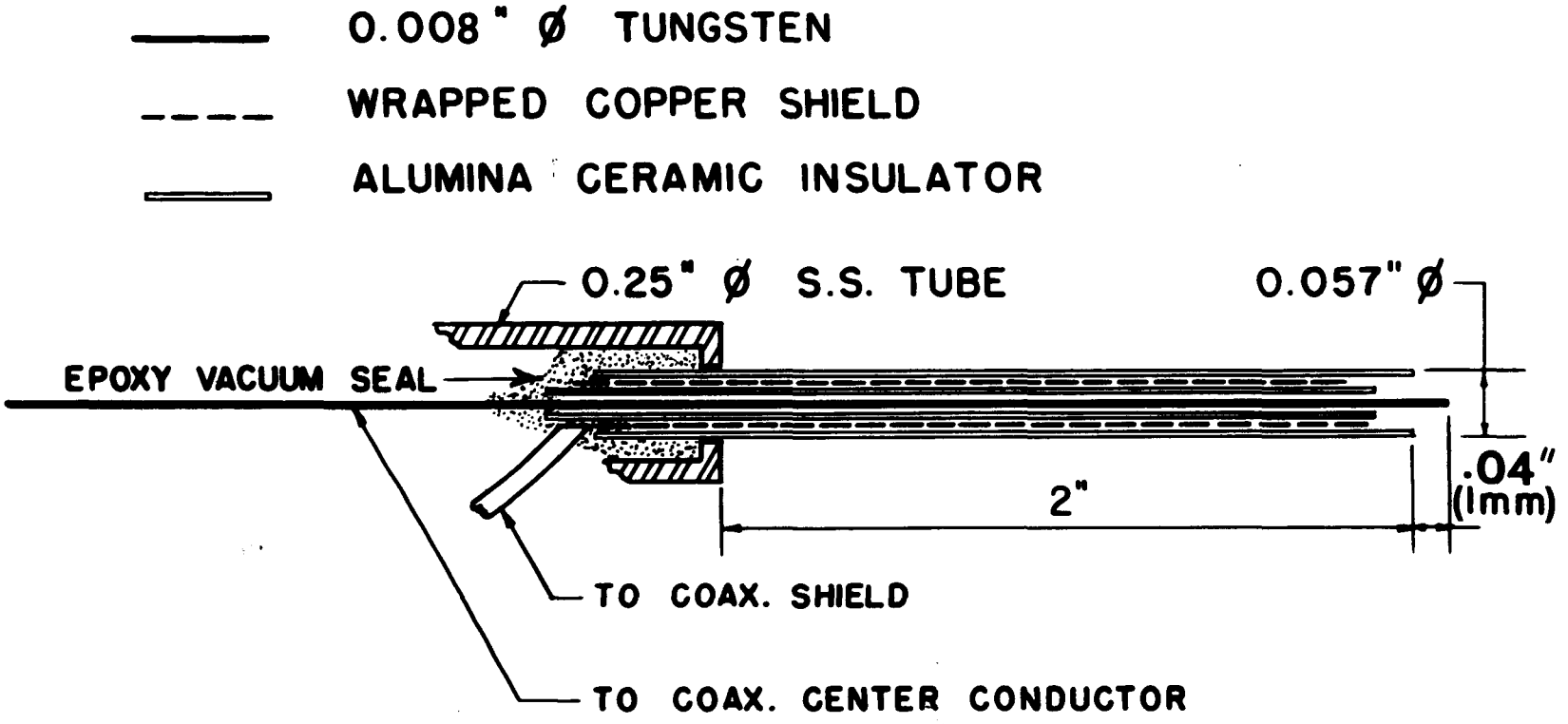

Figure 2-8 Construction of Langmuir Probe

the point of collection. 1/2 mm recession of the inner insulating tube helps prevent short circuit due to potassium deposit precipitated out of the plasma. The wire and foil shield are connected to the oscilloscope or meter via a coaxial cable to minimize noise and ringing.

The simplicity of the probes' construction and geometry belies the complexity of its theory, even in the case of a collisionless field-free plasma. This is due to the unavoidable disturbance of the plasma by the probe, creating boundary conditions whose effects have not been calculated with any great degree of rigor. Chen gives a review of the theory of probes in which analyses by Langmuir, Bohm, Lam and others are discussed[77].

In all experimental work reported here, the sheath thickness at the probe is small compared to the probe size, and the latter is small compared to the mean free path and ion Larmor radius. The effects of collisions shall be neglected and the effective collecting area of the probe is nearly equal to its geometrical area.

Discussion of probe utility begins with the potential-current relation of probe in plasma, known as the probe characteristic (Fig. 2-9). The reference point for potential is the grounded vessel that contains the plasma. The plasma is assumed to be collisionless

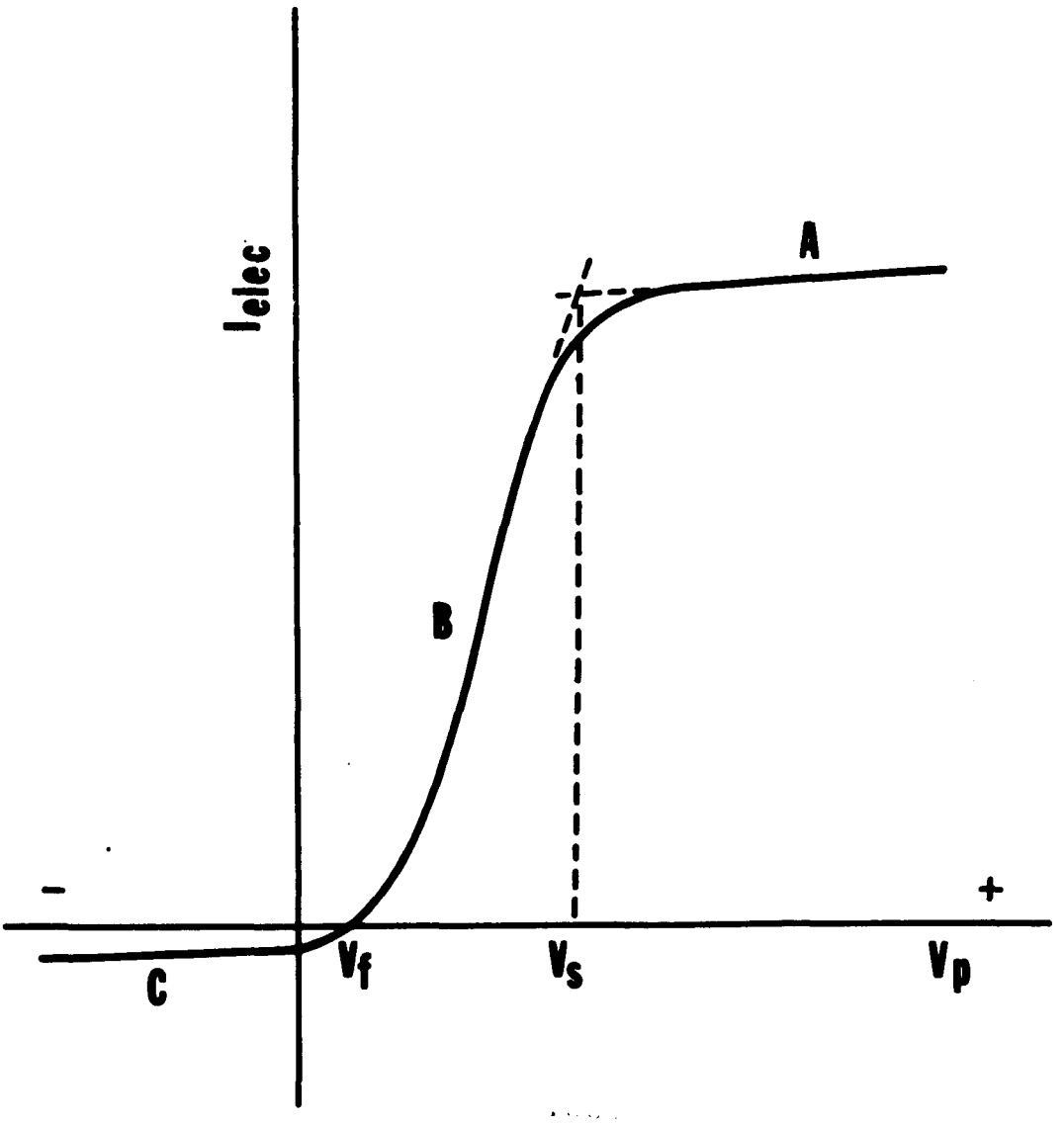

Figure 2-9 Typical Probe Current-Voltage Characteristic

and field-free, the point V_S is the plasma space potential, at which there is no potential difference between plasma and probe. There is no electric field near the probe, and collected current is due purely to thermally drifting particles hitting the probe. Since electrons are much more mobile than ions, current is mainly electronic. Biasing the probe more positive than Vs results in the formation of an electron-dominated sheath inside which electrons are attracted and ions are repelled. Outside the sheath, the plasma experiences virtually no electric field and is undisturbed by the probe. In region A ($V > Vs$), the collected current is overwhelmingly electronic, as V rises, more ions are repelled, the sheath grows in size, increasing the effective collecting area, and electronic current increases. Above Vs however, all ions but those in a miniscule high energy tail of the distribution are excluded. The sheath size grows slowly with V; hence, in this region, the slope of the curve is slight. This portion of the curve is called the region of saturation ion current. As V is lowered beyond Vs, more ions are picked up, and the net current decreases down to Vf, the floating potential. Here ionic pickup equals electronic pickup. An isolated probe assumes this potential in plasma. The region B ($Vf < V < Vs$) is a transition region between electron and ion saturation. As V is lowered beyond Vf (region C), more

electrons are excluded, and the current becomes virtually all ionic. The plot flattens out as it does in region A, for the same reason.

In region B, the current is predominantly electronic, and if the electron distribution be Maxwellian, the collected current would be proportional to exp(-eV/kTe), where Te is the electron temperature. The slope of a plot of Ln I vs V would be -e/kTe, from which Te may be gotten.

The assumption of large Larmor radius is not fulfilled by electrons with any magnetic field used in these experiments, so that simple probe theory would be invalid for electrons[77]. Plasma density is gotten by measuring saturation ion current, for which a simple theory exists.

It is well known that the current of a species incident on any surface of area A is $1/4ne\bar{v}A$, where n is the density of that species and $\bar{v}$ its mean velocity[78]. This equation is valid where no field is present. For a cylindrical probe at potential V, and ions with incident kinetic energy $\mathcal{E}$, it can be shown that this current is increased by a factor $\sqrt{1+eV/\mathcal{E}}$, or

$$I_{sat} = \frac{1}{4} n e \bar{v}_i A \sqrt{1 + eV/\mathcal{E}} \qquad (2\text{-}1)$$

Now the sheath may be penetrated by electrons with their thermal energy. Equating this thermal energy with the potential induced at the sheath edge by this penetration at equilibrium, one obtains

$$V_s = \frac{kT_e}{2e} \tag{2-2}$$

It is well known that for a Maxwellian distribution $\bar{v}_i = \sqrt{2kT_e/m_i}$ in the absence of an electric field. The mean velocity of ions incident to this "charged sheath" is

$$\bar{v}_i = \sqrt{2/m_i\,(kT_i/3 + eV_s)} \tag{2-3}$$

The ion density is given by

$$n_i = n e^{-eV/kT_i} \tag{2-4}$$

where $\bar{n}$ is the undisturbed ion density. Further solution for Isat requires knowledge of the temperatures. One obtains ,

$$I_{sat} = 0.4\,An\sqrt{\frac{2kT_e}{m_i}}\,(T_i/T_e) = 0.01 \tag{2-5a}$$

$$I_{sat} = 0.38\,An\sqrt{\frac{2kT_e}{m_i}}\,(T_i/T_e) = 0.5 \tag{2-5b}$$

It is seen that Isat is not highly dependent on Ti.

Saturation current is read on a Keithley model

610B electrometer connected in series with a 90V battery and the probe. Floating potential is read on the same device with the probe connected directly to the input. (The input resistance of the electrometer switched to voltmeter mode is greater than 10^{14} ohms, assuring truly "floating" conditions.) The output of the meter is fed into a Y-axis input of a Moseley 136A two pen X-Y recorder. The X-axis is driven by the probe transport potentiometer, so that potential or current profiles are obtained.

Density oscillations are observed by biasing the probe to collect ion current, with the current passing thru a 1K resistor. The ac voltage developed across the latter is fed into a type 1A7 preamp. plug-in unit of a Tektronix 555 dual beam oscilloscope. The preamp output is also fed into a 1L5 spectrum analyser that essentially Fourier transforms the signal. The oscillation and its spectral density may then be observed simultaneously.

Part C - Plasma Camera

The plasma camera is perhaps the most useful diagnostic tool employed in these experiments[76]. It provides an instantaneous visual two-dimensional profile of the entire plasma column.

The camera is illustrated in Figs. 2-10 and 2-11. When the camera is not in use, the stainless steel flag acts as the column terminating cold plate. This protects the camera from potassium coating by prolonged ion bombardment, and from thermal damage due to prolonged electron bombardment. When the camera is in use, a 25 line/inch, 50% transmissive, 0.003 inch thick stainless steel mesh terminates the column. An inch behind the mesh screen is a glass disc, 2 3/4 inches in diameter, 1/2 inch thick, coated on one side first with P1 or P11 phosphor, then with aluminum, so that the aluminum layer faces the screen. The aluminum outer coating excludes visible light from the incandescent cathode and filaments, and ultraviolet light from the plasma. This coating is 0.3 - 0.5μ in thickness, being just thick enough to be opaque.

When taking a picture, a less-than-a-microsecond 4 - 12 kv pulse is imposed between the aluminum coat on the glass disc and the screen. If the latter be positively biased with respect to ground, electrons in the sheath of the screen will be accelerated through the aluminum layer onto the phosphor, causing it to scintillate, yielding an "electron picture" (Fig.2-12a). If the screen be negatively biased, it is the secondary electrons produced by the ions in the sheath bombarding the screen that penetrate the aluminum coating, yielding an "ion picture" (Fig.2-12b). Note that the lines in the screen are bright in the ion

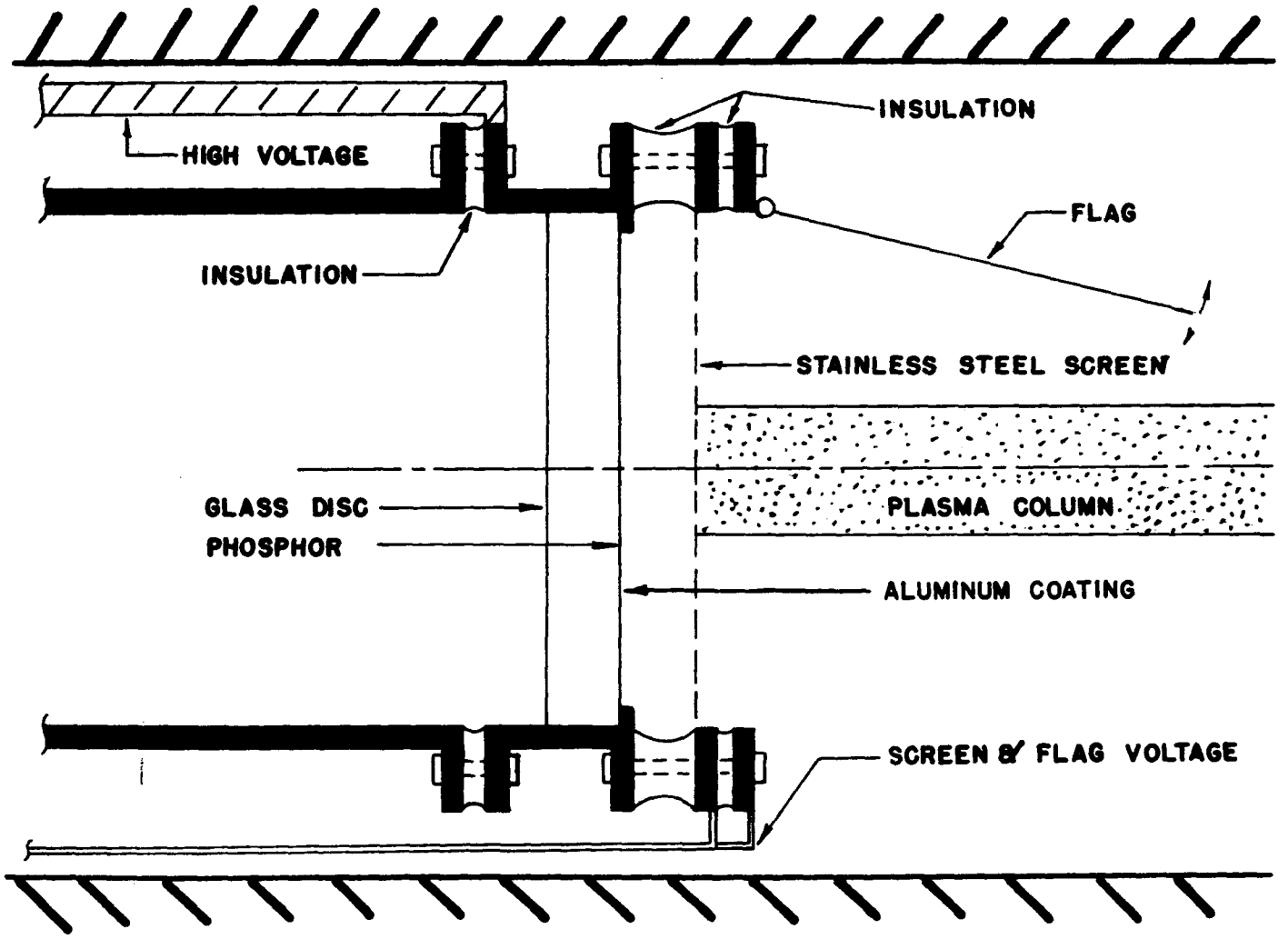

Fig. 2-10 Schematic of Plasma Camera

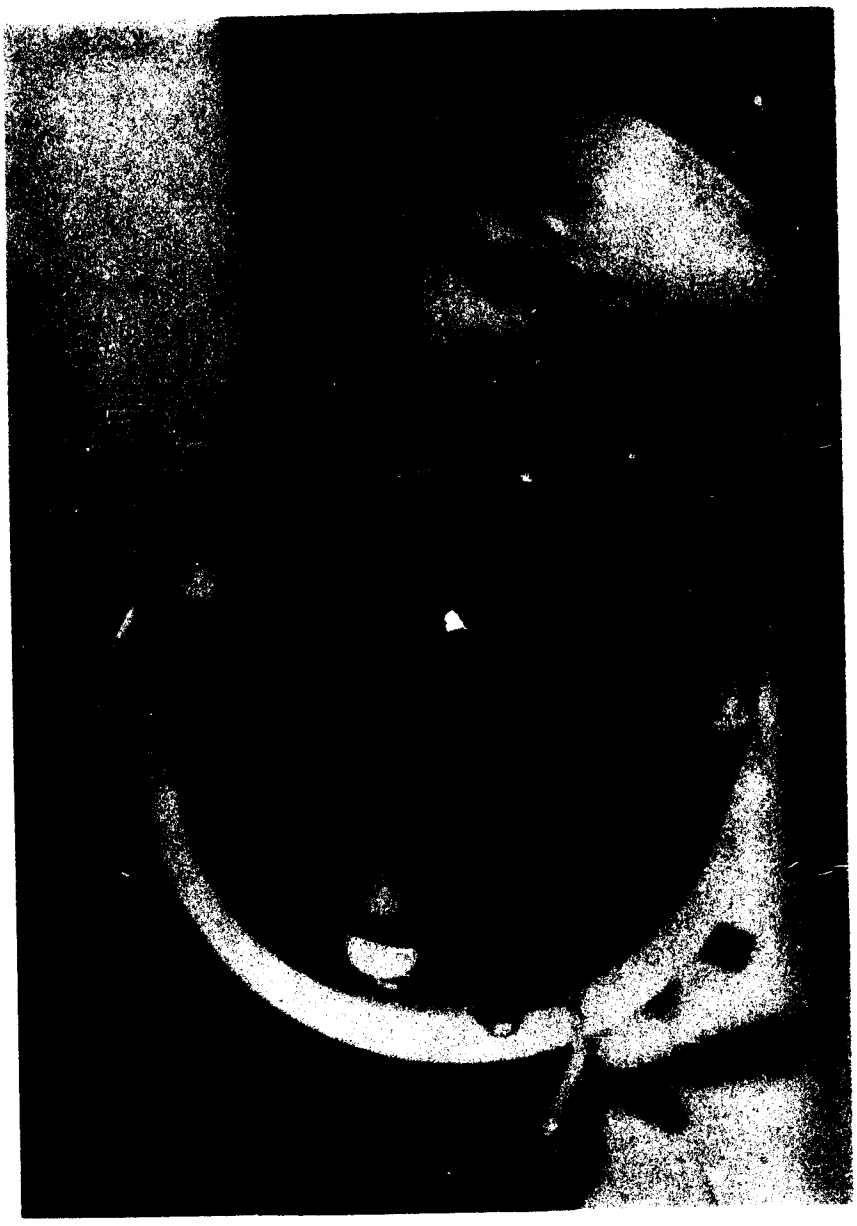

Fig. 2-11 The Plasma Camera

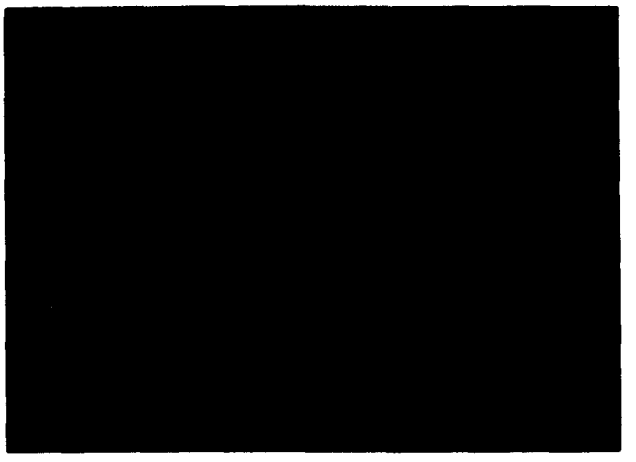

Fig. 2-12a Plasma Camera Photograph of an Electron Distribution with Probe Shadow.

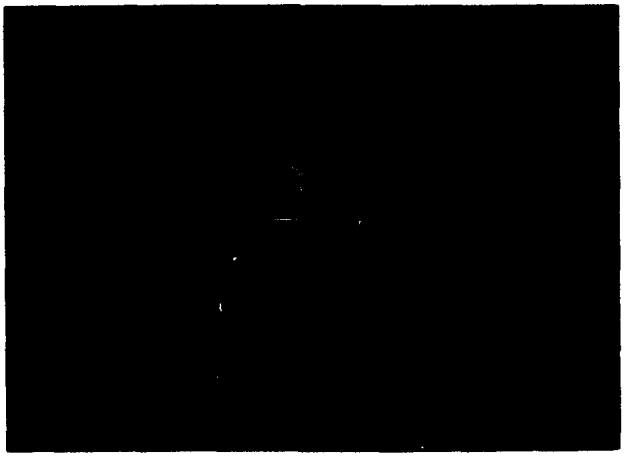

Fig. 2-12b Plasma Camera Photograph of an Ion Distribution with Probe Shadows.

picture due to secondary emission, while in the electron picture, the holes are bright, due to direct electron bombardment. An optical camera (Graflex with Polaroid back) records a 1:1 scale photograph of the scintillation. Observation of probe shadow (Fig.2-12) proves the spacial accuracy ($\pm$ 1/2 mm) of this photographic technique. The probe shadow appears larger in the ion picture because the ion Larmor radius, (0.015 mm at 1 kG) is much smaller than the probe diameter.

Part D - Diffusion Measuring Devices

Two devices are used to estimate transverse current, each in a different way. The radial particle collector[7,8] measures transverse current directly, while the terminal particle collector[20,72] measures loss of plasma along the column, this loss being assumed to be almost entirely due to transverse diffusion.

1) Radial Particle Collector

The transverse diffusion coefficient $D_\perp$ is obtained from the relation $D_\perp = j_\perp / dn/dr$. dn/dr is obtained by drawing a slope on a plot of plasma ion current profile from a radial sweep of the Langmuir probe. The transverse flux $j_\perp$ is obtained using the radial particle collector. As shown in Fig.2-13, it consists of a set of 3 parallel brass plates, the outer two being electrically connected. The small 1 1/2 mm

gap minimizes the collection of longitudinal current. It is placed about 4 or 5 column radii from the center of the plasma to prevent its influencing the latter.

The current-voltage characteristics of the collector are shown in Fig.2-14. In region I, the effect of the applied potential extends only to the edge of a thin sheath formed around the plates. In region II, the sheath thickness is larger and the current collecting area grows with increasing V. In region III, the potential is sufficiently high so that the sheaths overlap. Almost complete separation occurs, and the plates collect ion and electron saturation currents. The device is operated in this region (V = 22 1/2 volts). In operation, the presence and biasing of the collector has no discernible influence on any plasma parameter.

2) Terminal Particle Collector

The transverse flux may also be known by measuring the plasma flux along the colum. Let j_1 be the plasma flux out of the cathode and j_2 the plasma flux into the cold plate. If volume recombination is small compared to plasma diffusion, the difference between j_1 and j_2 is due almost exclusively to diffusion. It is assumed that the plasma column is axially symmetric and that $D_\perp$ varies very little along the column length z. The loss of flux due to diffusion in the loss per unit area $D_\perp$ dn/dr (Fick's law), times the columnar area $2\pi a z$, where a is the cold plate radius. We have then

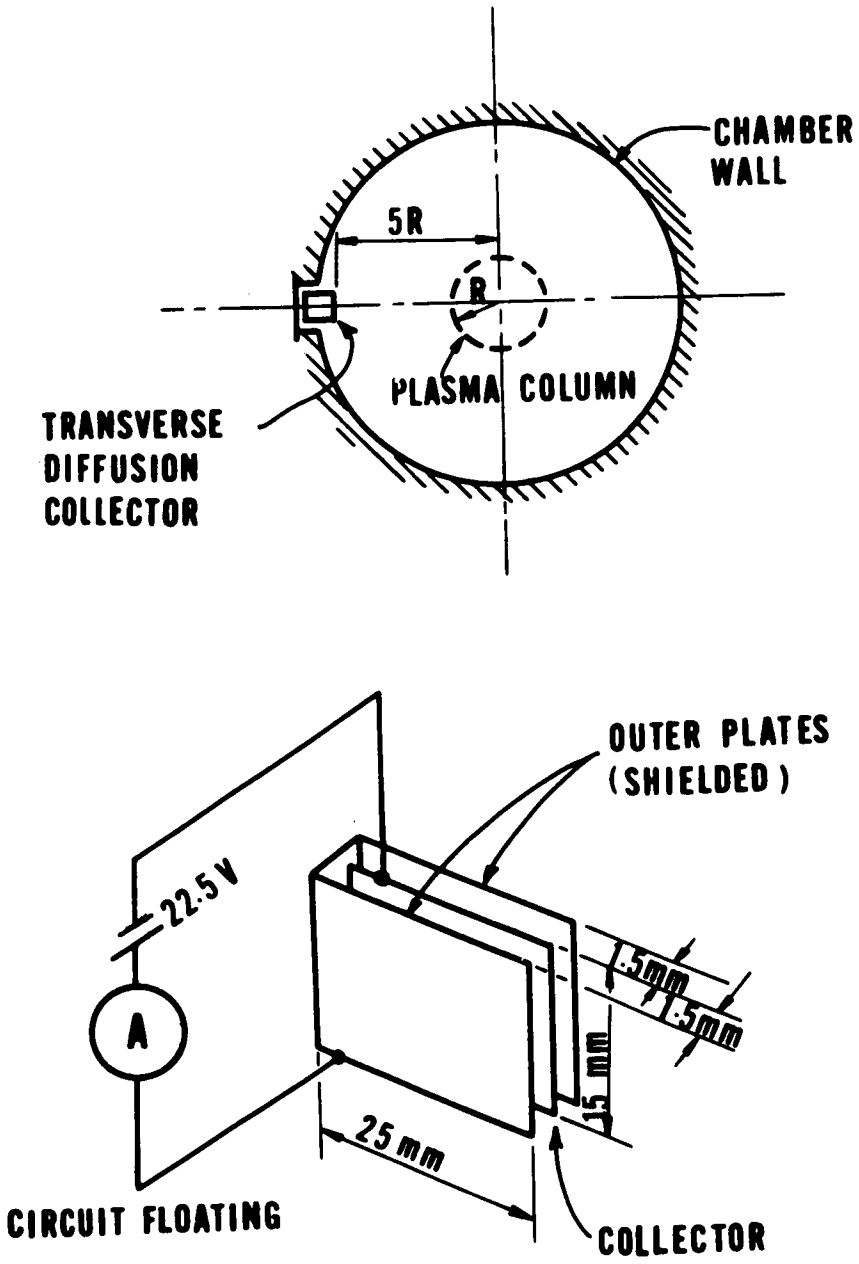

Figure 2-13 Transverse Diffusion Collector

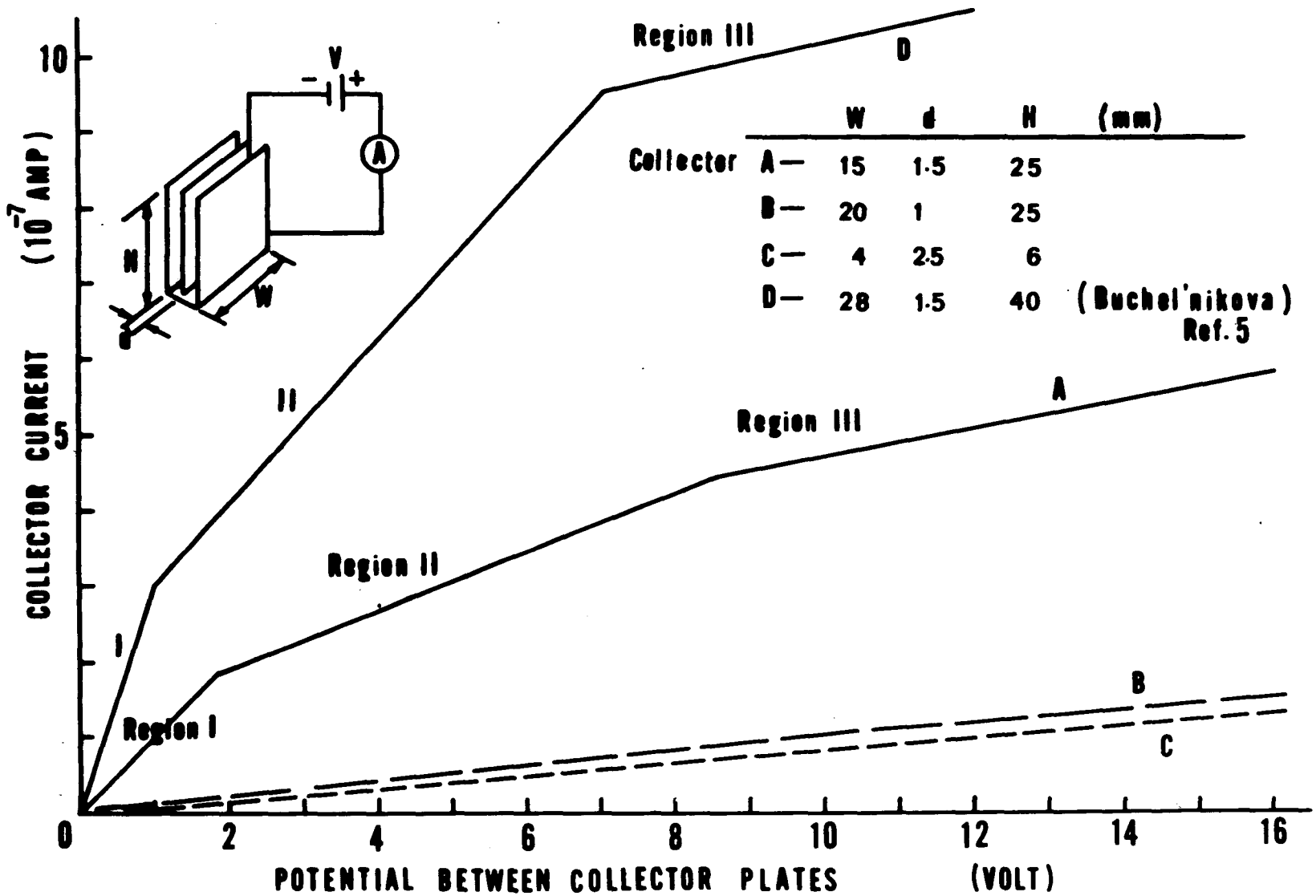

Figure 2-14 Diffusion Collector Current-Voltage Characteristic

$$j_1 = j_2 + j_\perp$$

where

$$j_\perp = D_\perp \frac{dn}{dr} 2\pi a z \tag{2-6}$$

If the column length is changed slightly while j_1 remains constant, then

$$\Delta j_1 = 0 = \Delta j_2 + D_\perp \frac{dn}{dr} 2\pi a z \tag{2-7}$$

if Δz is small compared to z and dn/dr remains constant as z is changed, we may make the approximation

$$D_\perp = -\frac{1}{2\pi a}\left(\frac{dn}{dr}\right)^{-1}\frac{dj_\perp}{dz} \tag{2-8}$$

the saturation current I collected by the end plate is j_2/e. Then we have

$$D_\perp = -\left(2\pi a e \frac{dn}{dr}\right)^{-1}\frac{dI}{dz} \tag{2-9}$$

and we can identify $-1/(2\pi a e)\ dI/dz$ as $j_\perp$. dI/dz is obtained by sliding the collector along the machine axis and noting the collector current change.

The collector itself consists of a stainless steel disc, 1 inch in diameter perpendicular to the column, 3/8 inches in front of a brass capped cylinder of 1 5/8 inch outer diameter, 2 inches in length. A

3/4 inch diameter, 3/8 inch long boron nitride cylinder insulates the disc from the brass cylinder. In effect, this affords the use of two cold plate areas and enables comparison of plasma density in inner and outer regions.

Part E - Summary

The experimental apparatus, including diagnostic tools and techniques have been described in this chapter. A great variety of limiter sizes and shapes, filamentary configurations, and an impregnated cathode emitter have been used in these experiments. The plasma camera affords a view of the plasma column over a time span of less than a microsecond with $\pm$ 1/2 mm spacial resolution. The Langmuir probe is used to obtain radial profiles of plasma density, potential, and oscillations. Transverse current due to plasma diffusion is measured with radial and terminal particle collectors.

CHAPTER III

EXPERIMENTAL RESULTS

Previous experimental investigation of cells in the CCNY Q-machine has dealt with their discovery, the magnetic fields at which they occur, and their association with increase in plasma density and suppression of edge oscillation.

The present work includes an investigation of conditions at which cells occur. A mechanism for these cells has been found empirically. The effect of confinement of a plasma column of an enveloping beam of energetic electrons is studied. Of considerable interest is the correlation of the depth of a potential well across the column with the ion density and transverse diffusion.

Part A

The experimental work reported here centered upon a thorough investigation of plasma cells in a Q-machine via operation with a great variety of conditions, configurations and geometries of the assemblies within the Q-machine.

Part B

Effect on plasma confinement (transverse current, transverse diffusion collector current, and plasma density) of a tubular beam of energetic electrons enveloping a conventional plasma column. Electron beams with both large and negligible transverse energy were used, in single and double-ended modes.

Part C

Experiments and observations that serve to complement A and B.

Part A - Plasma Cells

1) Cell Generation

The following is a description of experimental runs in which cells were observed.

Operating conditions

Limiters - Tantalum (Ta) - Circular apertures of 1/2 - 1 1/8 inch diam.

Boron Nitride (BN) 3/4 inch diam. aperture.

Filament-cathode potential - 0.4 - 2.2 kV

Cathode temperature 1300 to 2500° K

Endplate bias -300 - +300 V

At fields of 850 Gauss and above, the plasma column, as seen in plasma camera photographs (Fig. 3-1) is solid. The density profile

is roughly Gaussian (Fig.3-2). The floating potential profile is shown in the same figure (Fig.3-2). Edge oscillations ranging from 7 to 21 kHz were detected with the Langmuir probe. The observed signal is nearly sinusoidal; the spectrum analyzer detecting second, third, and sometimes higher harmonics. When the field was lowered to about 420 G, the column became hollow. Edge oscillations were seen, as before. At 320G, circular cells appeared (Fig.3-3) and the edge oscillations were suppressed below a low amplitude turbulent background. Ion density (Fig.3-4) and collector current rose (Fig.3-5). Density and floating potential profiles at 200G are shown in Fig.3-6. The cell diameters increased as B was lowered, and the cells disappeared below 100 G. The column became solid and roughly Gaussian. Ion density and collector current dropped (Figs. 3-4, 3-5). Density profiles for several fields are plotted in Fig.3-7. The cell diameter was found to vary as the square root of the filament-cathode potential (Fig.3-8).

Experimental runs have been made with a boron nitride (BN) limiter of similar aperture, and with a Ta limiter atop a BN limiter of the same and of larger diameter. Only slight quantitative differences from the above sequence were observed.

The effect of neutral flux was observed by operating under the above conditions with no neutral flux. The same phenomena were observed, the major difference being a 50% decrease in ion density

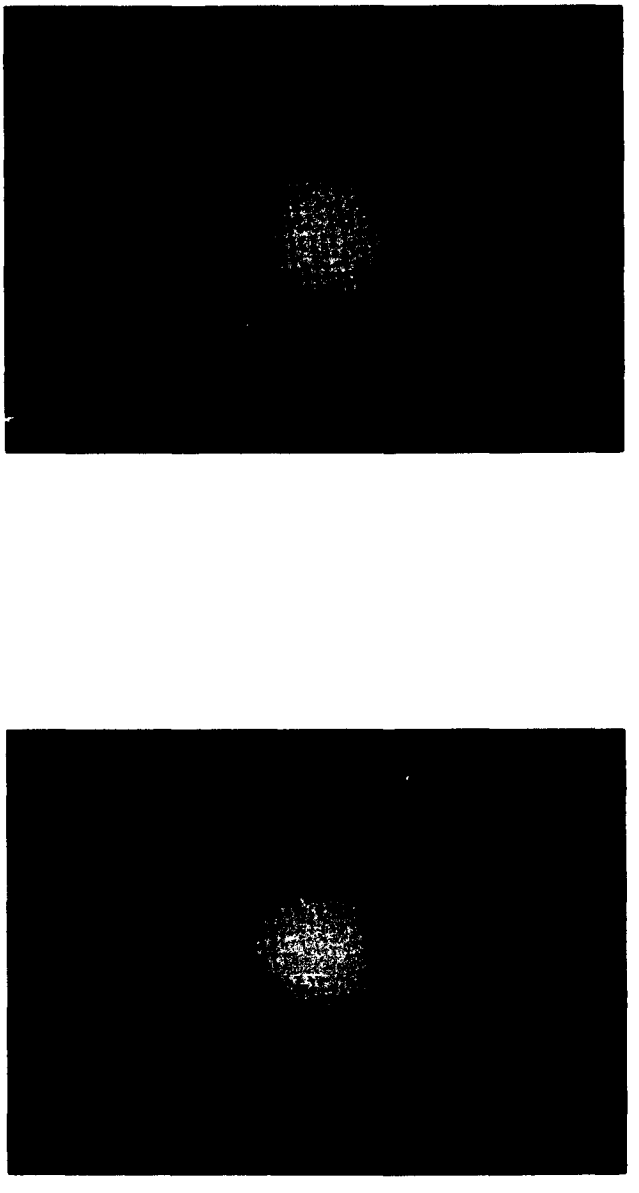

Fig. 3-1 Photographs of Column Above 1KG.

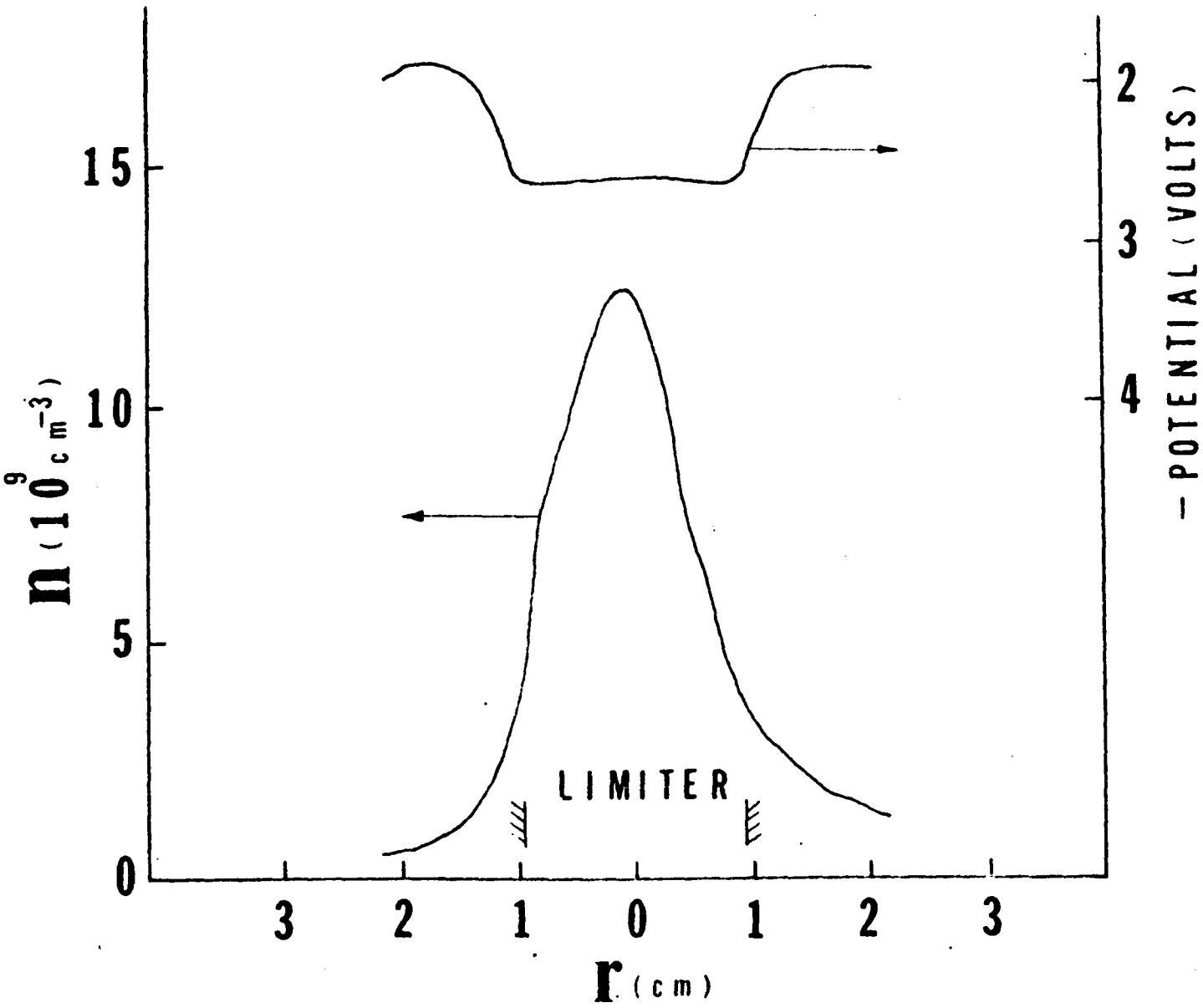

Fig. 3-2 Ion Density and Floating Potential Profiles at 850 G.

Fig. 3-3 Photograph of Plasma Cells at 200G.

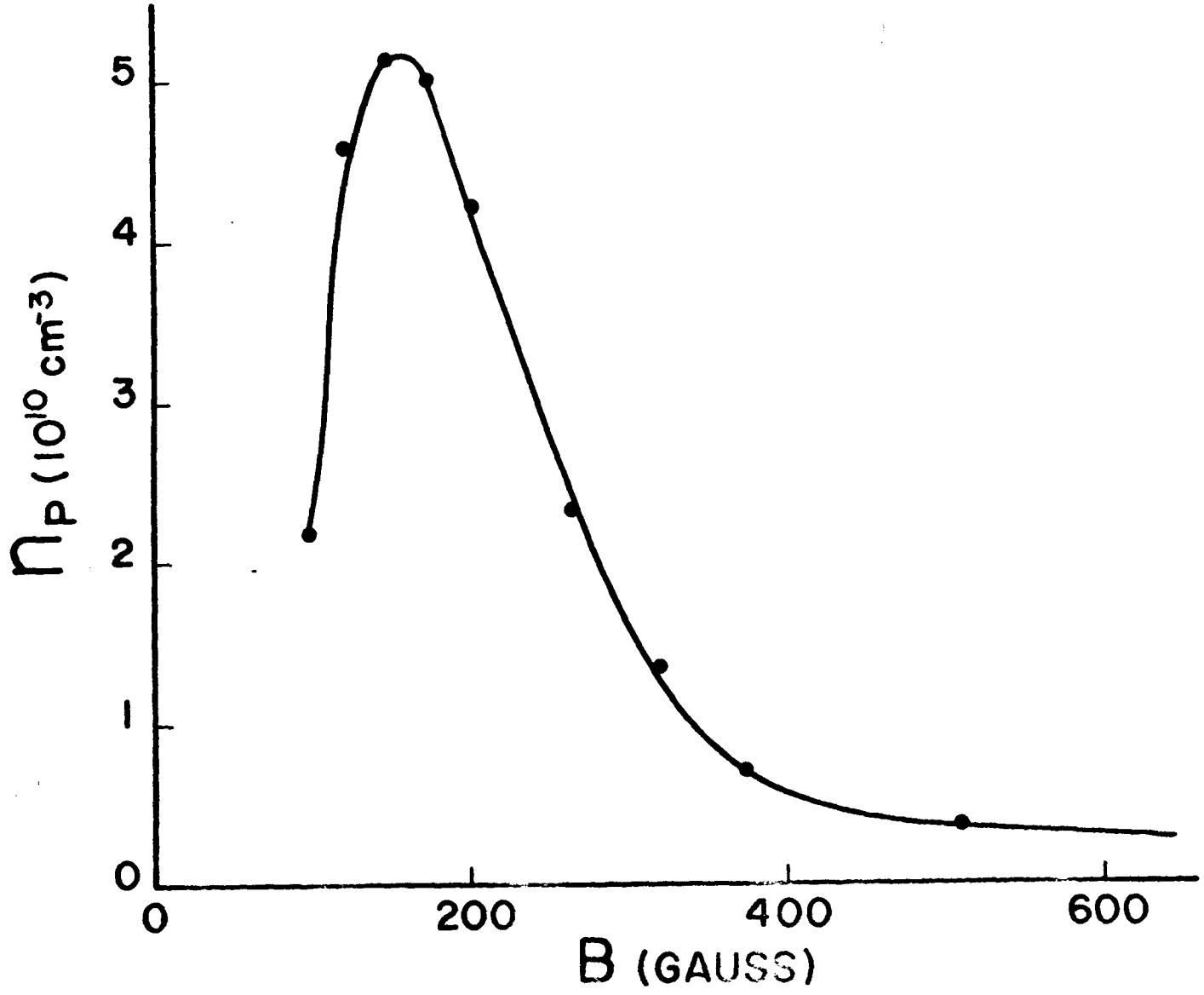

Fig. 3-4 Peak Ion Density vs. Magnetic Field

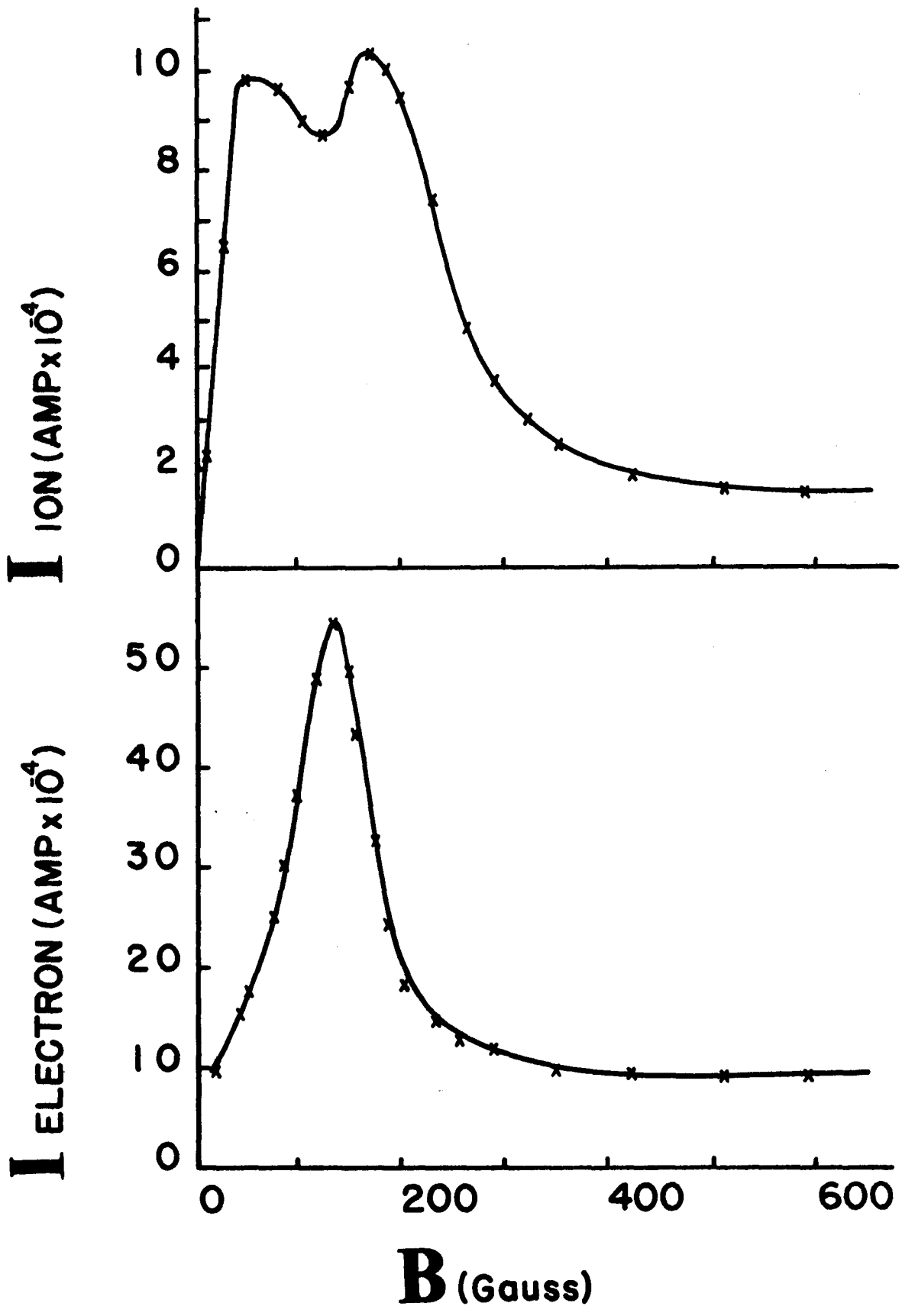

Fig. 3-5 Ion and electron collector current vs. magnetic field .

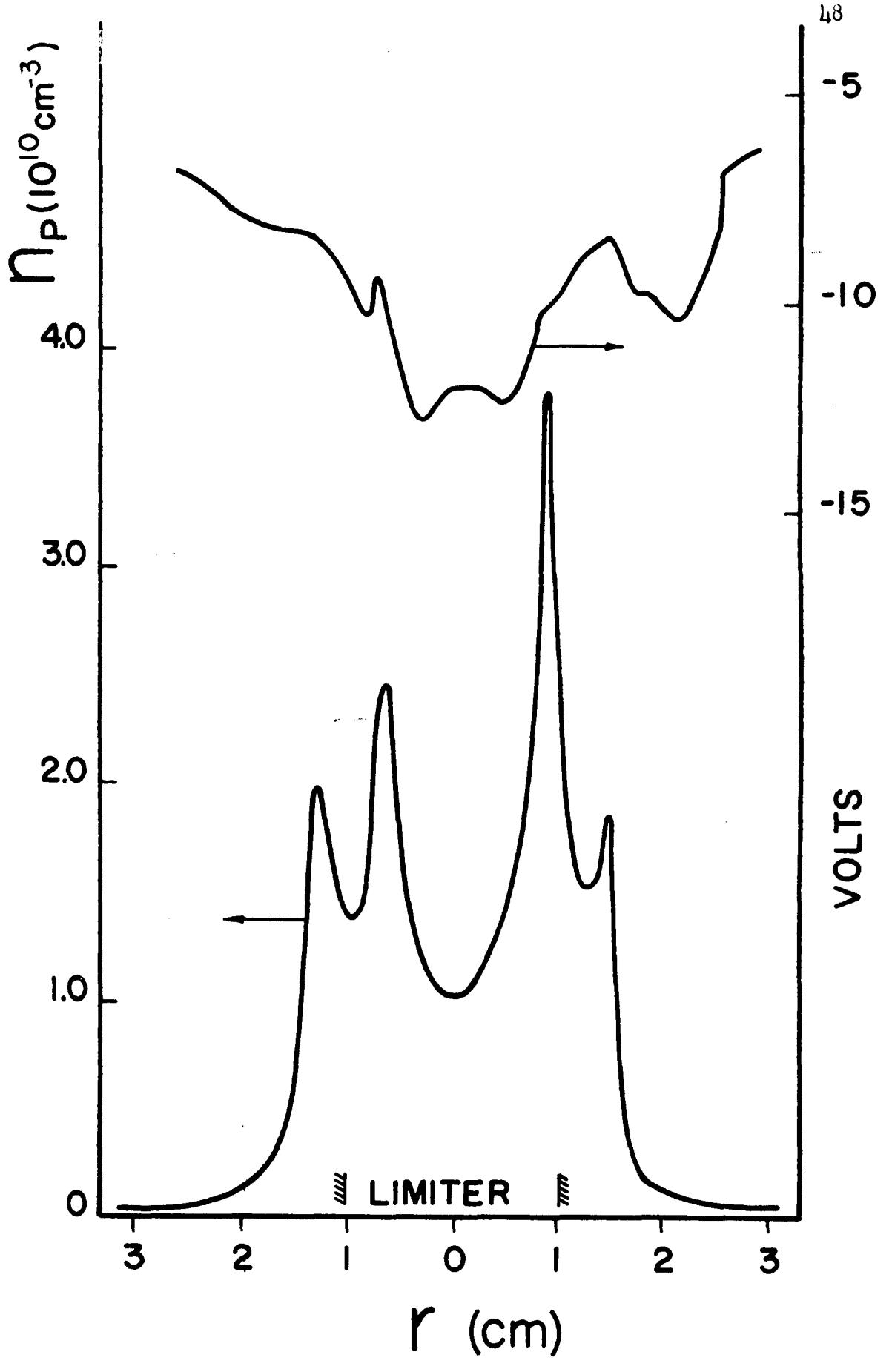

Fig. 3-6 Ion Density and Floating Potential Profiles at 200 G.

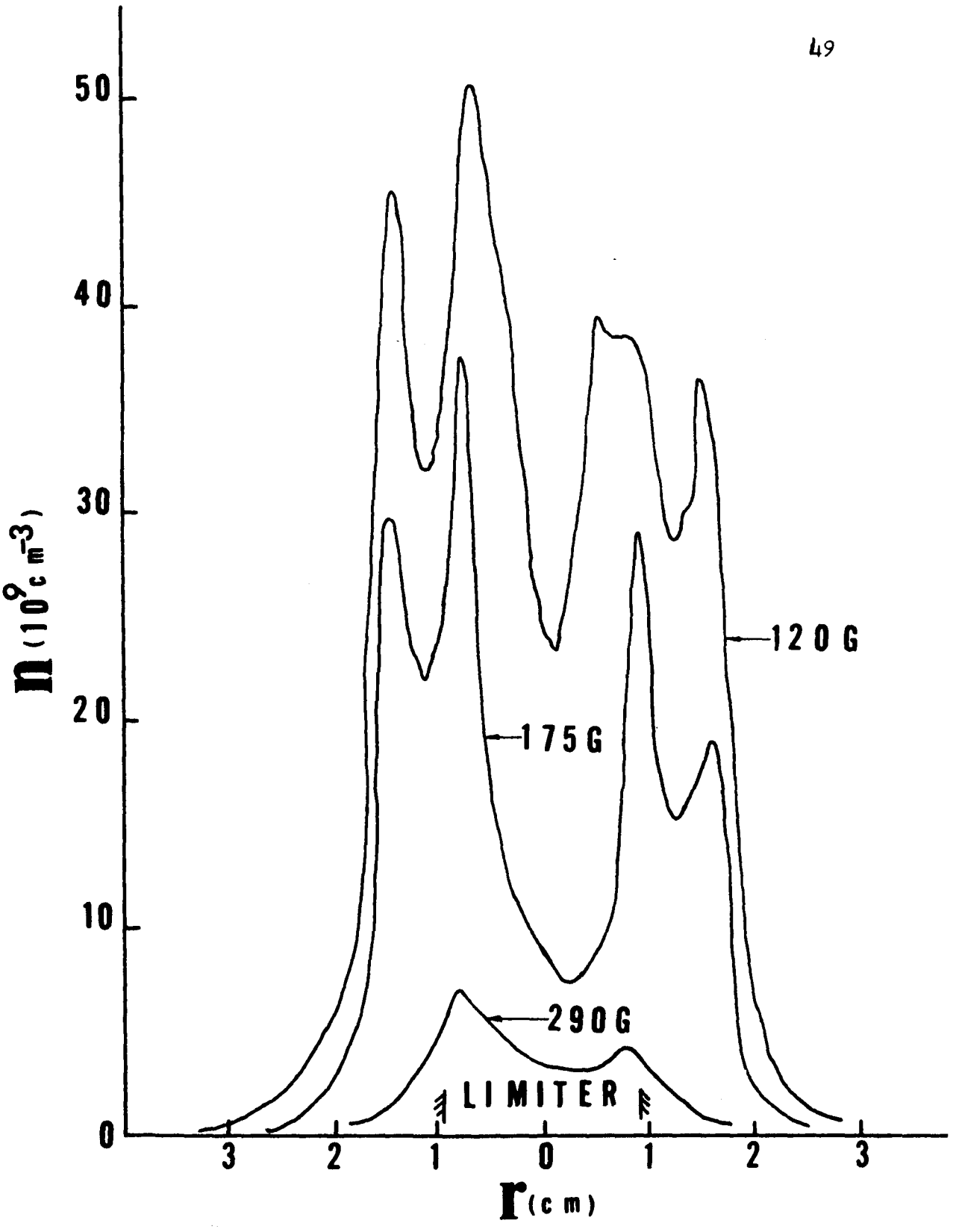

Fig. 3-7 Ion Density Profiles at Several Fields

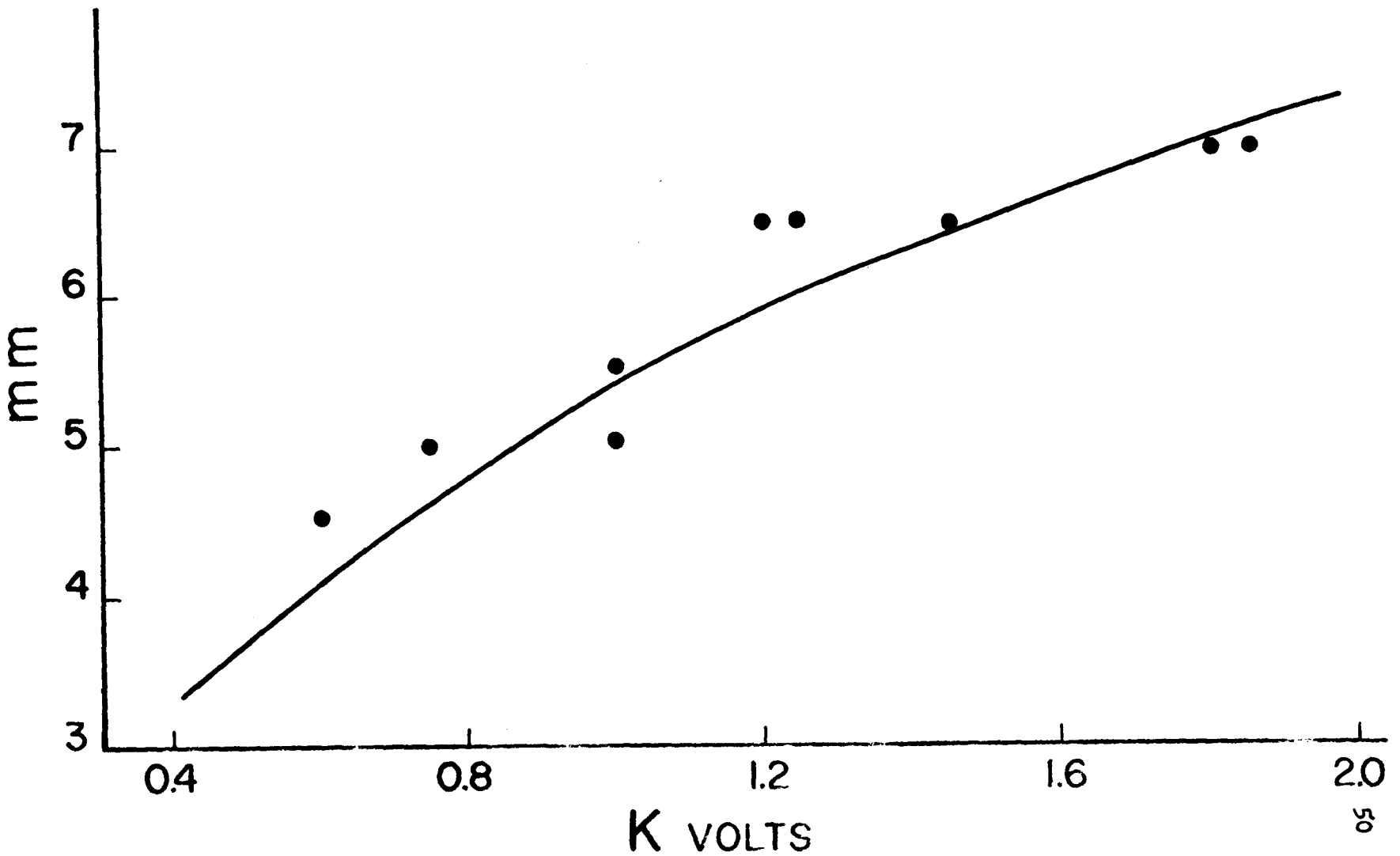

Fig. 3-8 Cell Diameter vs. Filament-Cathode Potential at 200 G

Line- Electron Larmor Radius
Points - Cell Diameter

throughout the range of magnetic field. The cellular structure was exactly the same. Cells were photographed with the cathode unheated and the identical filament-cathode potential. As long as the cells were perceptible, the magnitude of the filament current was not found to affect cellular structure or size. Cathode temperatures were varied from 2500° K to below 1300° K. The effect of cathode temperature is purely that ion density increases with this temperature.

The effect of cathode temperature gradient was investigated by tilting the cathode 11° with respect to the magnetic field axis. Photographs show a greater density variation, the side closer to the filament yielding higher density. The basic phenomena described above were noted.

The experiment was repeated with Ta limiters of differing circular aperture diameter (1/2 to 1 1/8 inch). The major observed difference is in variation of field at which onset of column hollowing and cells occur (280 - 420G). Cell diameter increases also with aperture diameter.

A small increase in cell size results if the limiter electrically floats. Imposition of a -1.5 kV limiter bias cuts cell diameter nearly in half. Cells may be eliminated by putting a negative bias on the limiter equal to the filament-cathode potential. Allowing the cathode to float has little effect on cell size. Cellular phenomena are

completely invariant to end plate bias.

Without the inner shield in place, the cells are a bit larger and appear less distinct as photographed.

All observations and data were basically unchanged when a 1 inch diameter tungsten wire loop was put in place of the usual zig-zag filament.

In order to investigate the possible influence of the 3 cathode support pins, a 1/4 inch thick 5/8 inch diameter steel disc was put in place of the cathode, supported from a strut downstream, assuring azimuthal symmetry in the electrode assembly. Cells were photographed with this configuration, their diameter varying with field and filament-cathode potential in the usual way. When the disc was moved upstream, its upstream surface flush with the limiter, electrons from the bombarding filament did not have sufficient transverse energy to create cells, and none were seen in photographs.

The augmented filament, described in the previous chapter (II-A3a) was designed to inject electrons at the column periphery and raise the onset field for cells. This was accomplished; cells, 2 mm in diam., were photographed at 850 G.

With the fully heated outer filament in the electrode assembly, cells were seen at fields up to 2.4 kG (diameter 1/2 mm). The observed phenomena were seen to depend on which filament emitted the

greater current and dominated the space within the assembly. With the inner filament predominant, the phenomena were as those produced by the inner filament alone. When the outer filament predominated, the column became hollow, even at fields above 500G, with numerous cells or bright spots seen in the photographed ring. Cellular sizes are smaller than those of the inner filament at equal fields and filament-cathode potentials.

Cells were photographed with the Ta limiter of 0.675 inch x 0.075 inch slot aperture in place. The cell diameter varies with field and filament-cathode potential the same way as with a circular aperture. Photographs show only 2 cells at the slot ends.

Shortening the column by as much as 8 inches leaves ion density, collector current, cell size, and column structure virtually unchanged. No rotation of the column is shown in photographs. Photographs were taken with the camera screen less than 1/4 inch away from the 3/4 inch aperture of the Ta limiter. The cathode was unheated. Cells were observed, their onset occurring above a critical filament-cathode potential: 1.4 kV at 375 G, 0.4 kV at 200 G.

2) Other Single-ended Runs

Insertion of the electron-blocking BN shield about the cathode (Fig.2-7) changes the plasma column and phenomena radically. Ion density and collector current diminish with magnetic field (Fig. 3-9),

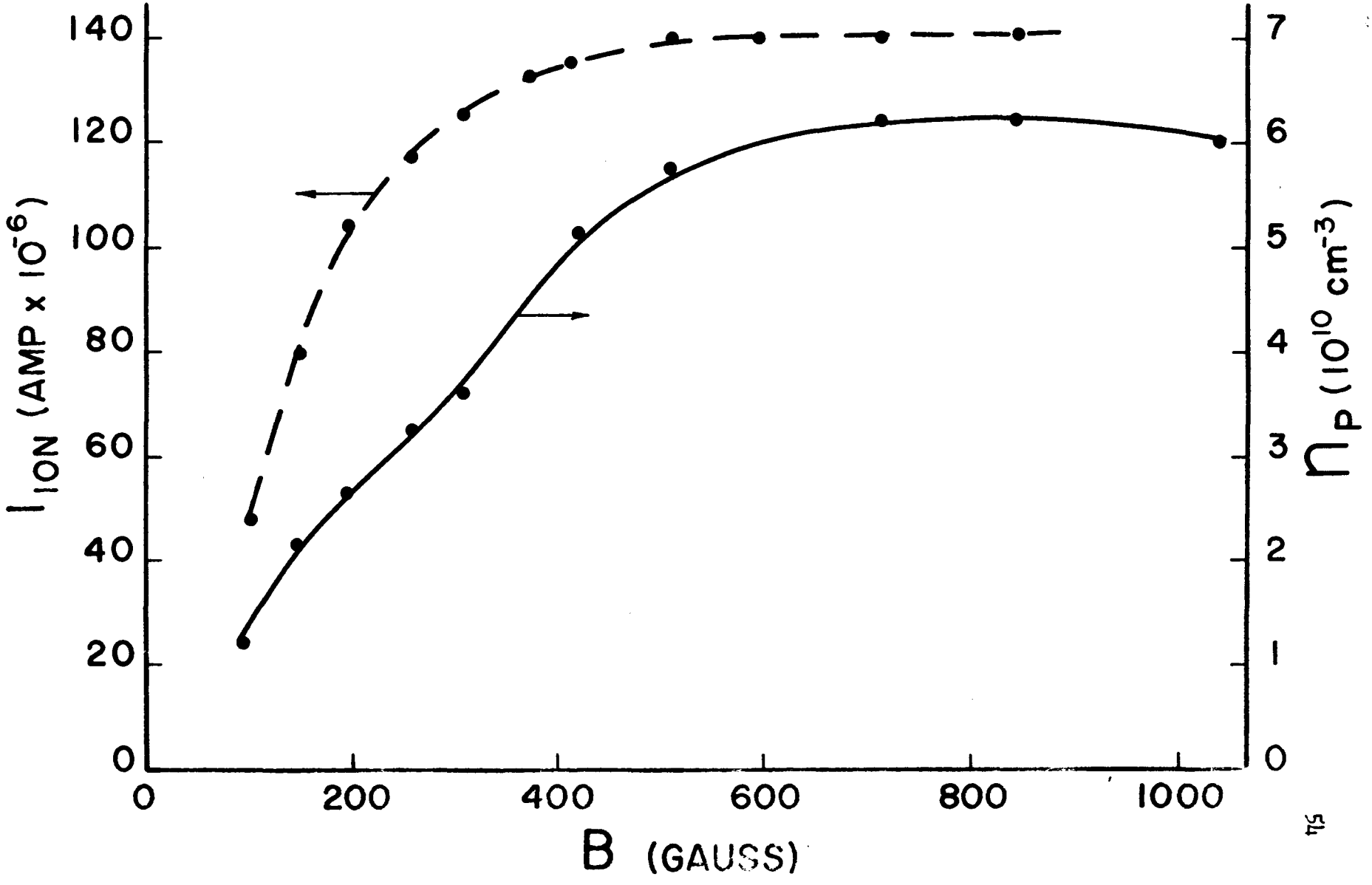

Fig. 3-9 Peak Ion Density and Ion Collector Current vs. Magnetic Field
n_p - Solid Line I_{coll} - Broken Line

and are generally smaller throughout the range of magnetic field used in these experiments. The column remains solid nearly throughout this range, becoming hollow below 100 G. No cells appear in any photograph. Edge oscillations, similar to those observed in the shieldless runs, persist down to 200 G.

Photographs were made of electron beams created by employing the perforated Ta limiter (II-A3c) in place of the tungsten hot plate. A circle of spots was seen. Variation of limiter-filament bias and magnetic field served but to focus and defocus the spots.

The impregnated cathode emitter (II-A3a) was placed in the electrode assembly behind a Ta limiter of 1 1/8 inch circular aperture and the 1 inch diameter tungsten hot plate so as to allow a tubular beam of electrons, about 1 1/16 inches in diameter to be emitted. This emitter is biased 1-2 kV below ground as are the filaments. Photographs taken at fields of 50 - 2400 G are similar, showing a ring with hot plate support shadows. Oscillations of 23 - 340 kHz were observed in the beam, the frequency rising with cathode temperature, seemingly independent of ion density or magnetic field.

When a limiter of 3/4 inch aperture was substituted for that of 1 1/8 inch aperture, and the hot plate lowered to its usual position, cells were seen, their diameter varying with emitter-plate potential and field in the usual way.

3) Double-ended Runs

To investigate the effect of imposing a tubular beam of electrons around an ordinary plasma column, the Q-machine was run double-ended with a BN electron shield in the plasma-generating side behind a 3/4 inch Ta limiter (Fig. 2-7).

With a similar arrangement on the non-generating side, observations showed conditions to be similar to those of a single-ended run, but with ion density approximately doubled due to the maintenance of hot end surfaces.

With the electron shield out of the non-generating side however, results are as if the atomic source were at this side; profiles and variation of parameters with field are entirely similar to those of the single-ended run first reported in this chapter. The profiles indicated a cellular structure in the column at appropriate fields. Density is greatly increased with the electron shield out.

Part B - Plasma Confinement

In this subchapter, results pertaining to plasma confinement (density, collector current, perpendicular current $I_\perp$, perpendicular diffusion coefficient $D_\perp$, radial electric field E_r, and depth of radial potential well) shall be presented. The radial particle collector has been used to measure $I_\perp$ in all modes and configurations of the Q-machine herein reported. The terminal particle collector was used

to measure transverse flux for a single-ended cell-yielding configuration. The structural details for both particle collectors and the derivation of $D_\perp$ from collector data are discussed in Chapter II part D.

1) Single-ended Cell-yielding Mode

Profiles of ion density for this configuration at fields of 50 - 1180 G are presented in Figs. 3-2 and 3-7. Note that at fields above 500 G and below 100 G (no cells) that the profile is roughly Gaussian and at fields for which cells have been photographed, the density profile is peaked at the cell rims. Variations of peak ion density n_p, radial particle collector current $I_\perp$, and $I_\perp/n_p$ with field are plotted in Figs. 3-4 and 3-10. $I_\perp$ and $D_\perp$ (measured with the radial particle collector) are minimal in the cellular range of fields, $D_\perp$ being 12 times as great at 510 G as at 200 G, whereas n_p and collector current are maximal in the cellular range of fields (Fig. 3-11).

Floating potential profiles indicate a potential well (for ions) across the column. Above 500 G, the well has a flat-bottomed form as in Fig. 3-2. The well spreads laterally and becomes somewhat rounded as the field is lowered. When the field is lowered beyond the threshold for electron emergence into the column with accompanying cells, the well steepens, and deepens to the double-humped shape in Fig. 3-6. The well depth increases as B is lowered, reaching its greatest depth

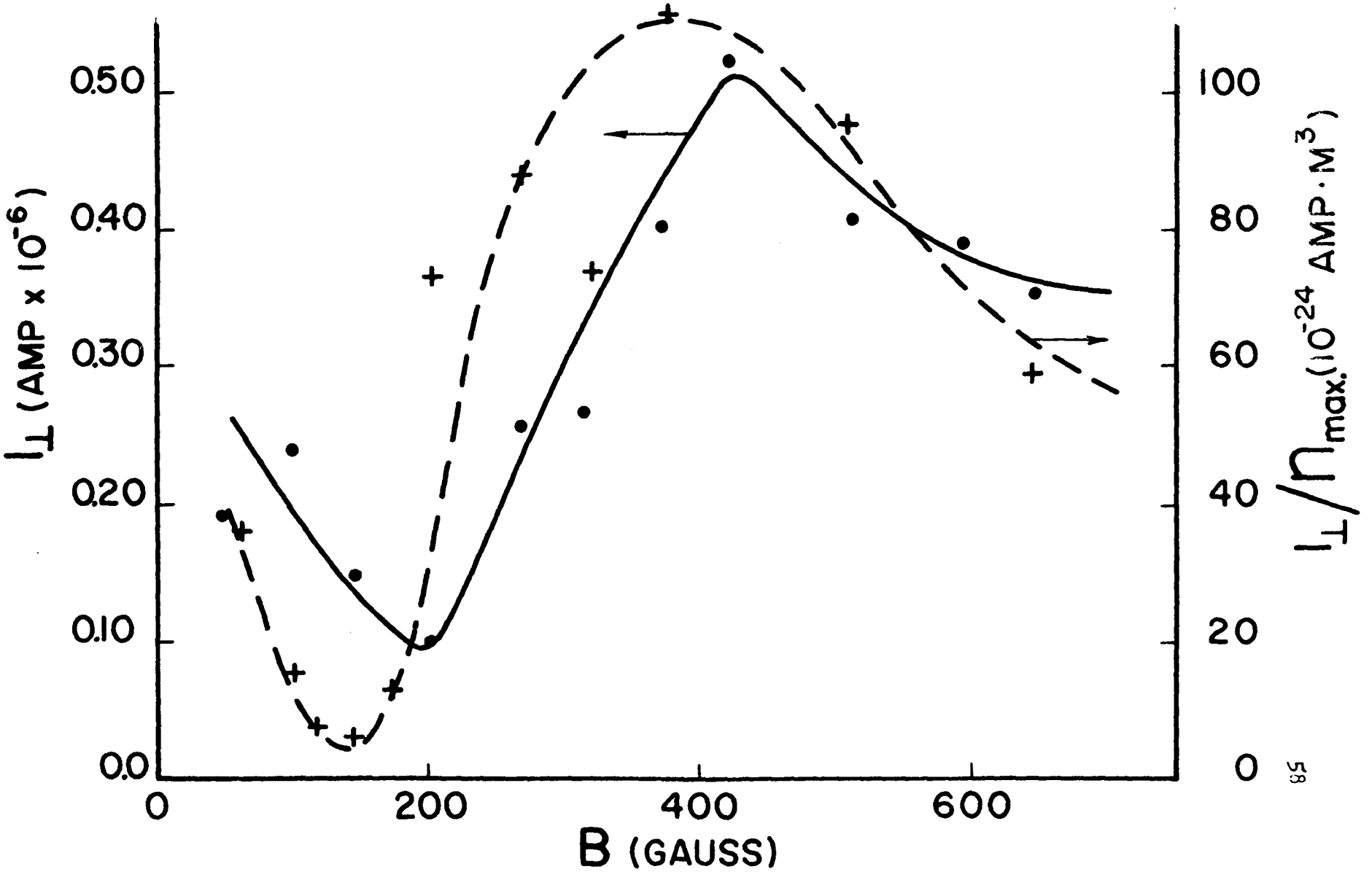

Fig. 3-10 $I_\perp$ and $I_\perp/n_p$ vs. Magnetic Field Solid Line - $I_\perp$ Broken Line - $I_\perp/n_p$

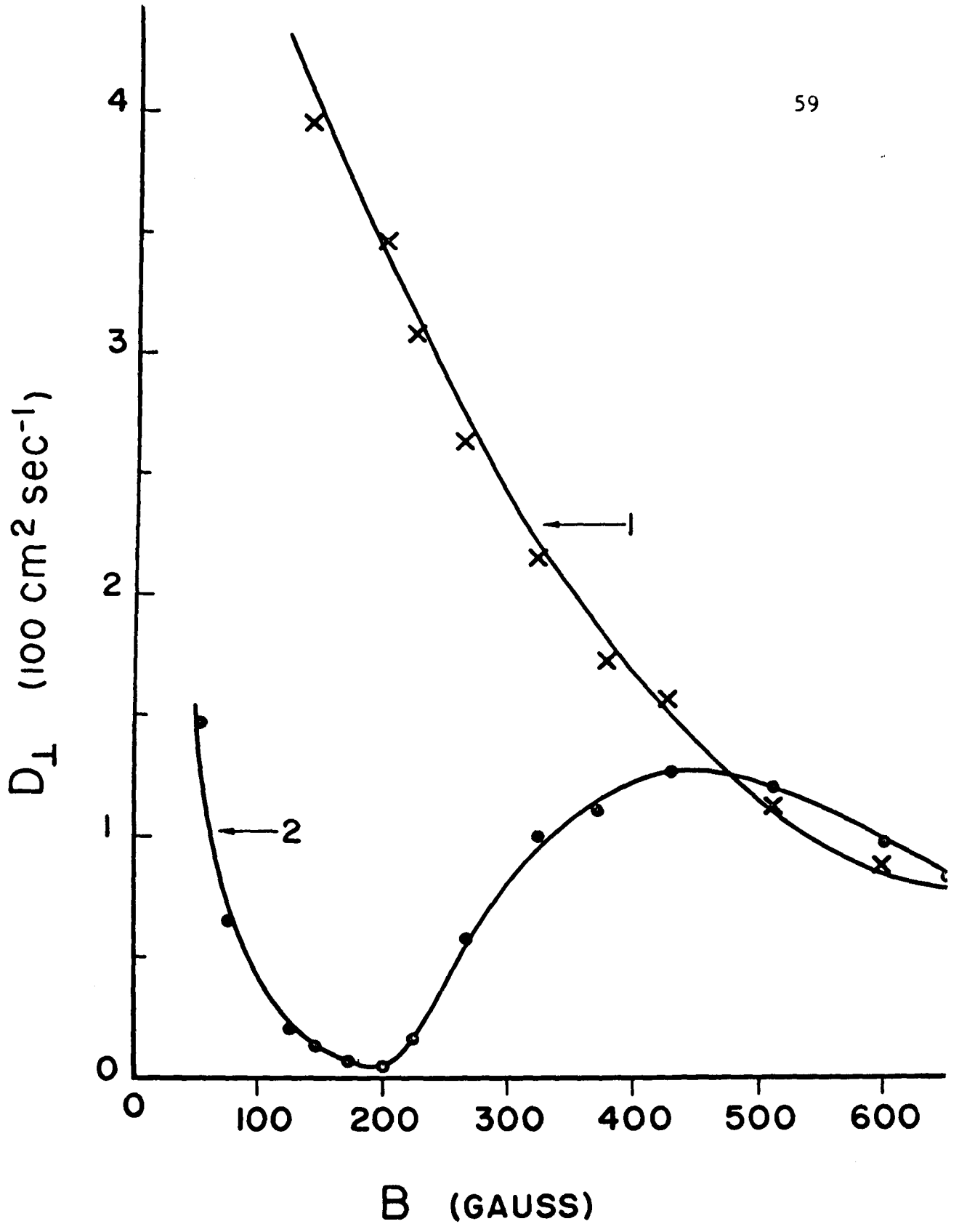

Fig. 3-11 $D_\perp$ vs. Magnetic Field Curve 1 - BN Electron Shield in Electrode Assembly

Curve 2 - Electrode Assembly in Cell-generating Mode

at fields for which the ion density is greatest (145 - 225 G range). Er = -dV/dr also increases sharply upon cellular onset. The well spreads out greatly and resumes a single-bottomed shape when the field is lowered below the cellular range. The well depth is plotted with magnetic field in Fig. 3-12. The well depth ranges from about 1/2 - 14 V; the wells are deepest with the cell-forming electron beam in the column. Note the inverse variation of $\triangle V$ with $I_\perp$ and $D_\perp$. The latter quantities negatively correlate quite consistently with the former.

The neutral flux was increased in order to increase ion density. Spreading of the potential wells did result, along with a drop in $\triangle V$ and Er as the density was raised. $I_\perp$ increased sharply as a result. At 200 G with a 3.3 V well depth, $I_\perp = 0.07 \mu A$, but with a 1.2 V well depth, $I_\perp = 0.24 \mu A$. Similar variation was found at 420 G and 850 G.

Data obtained from the terminal particle collector are quite revealing (Fig. 3-13). Note that the current collected by the inner (1 inch diam.) collector varies with field almost exactly as peak ion density, reaching a maximum at 145 G, where the cells are well developed. Below this field, as n_p and inner collector current drop, the current picked up by the annular outer collector (1 5/8 inch o.d., 1 inch i.d.) rises as the plasma column spreads out. The transverse plasma flux $j_\perp$, as obtained from terminal particle collector data varies with B in the same manner as $I_\perp$ obtained with the radial

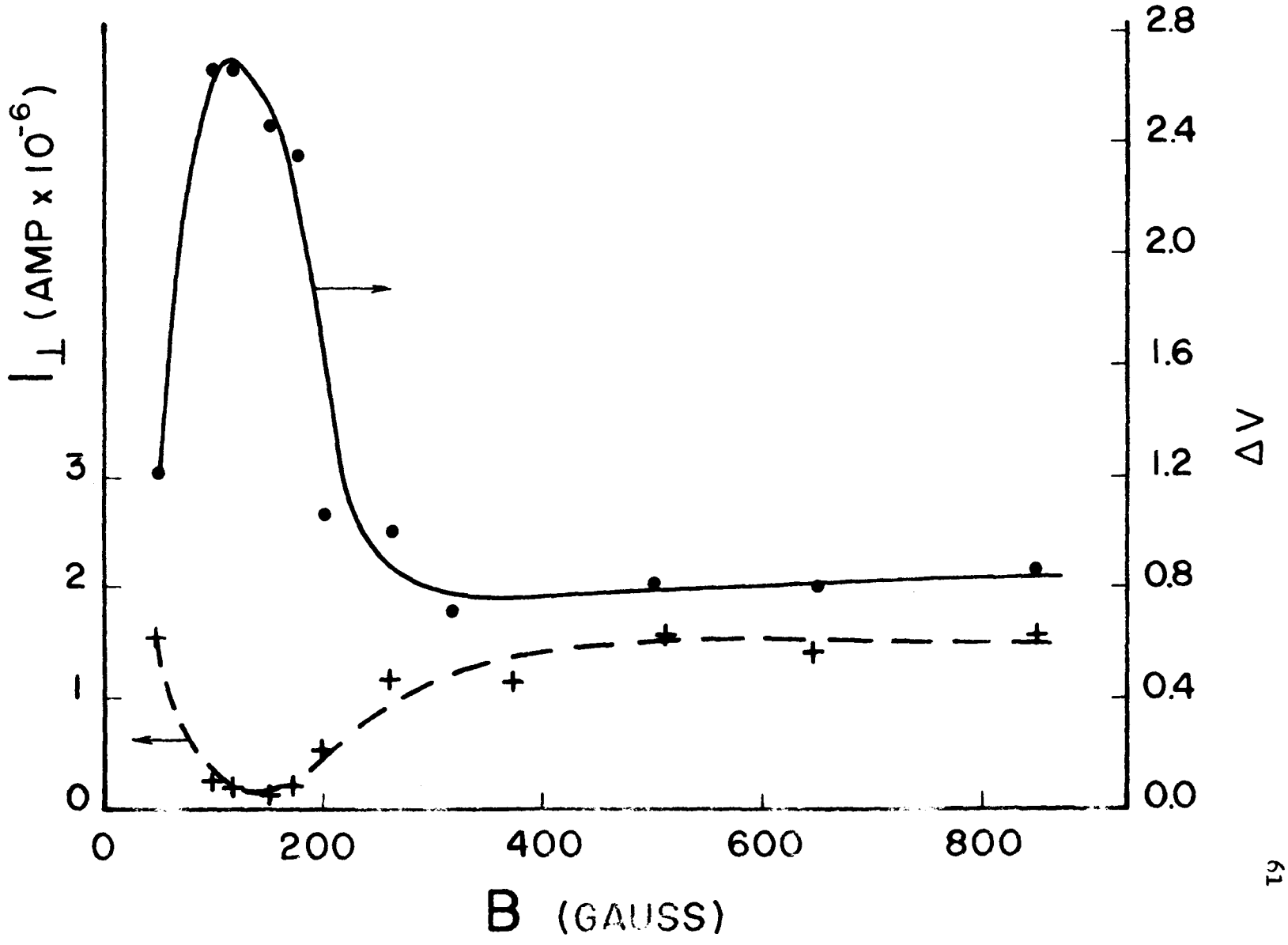

Fig. 3-12 $I_\perp$ and Well Depth ΔV vs. Magnetic Field Broken Line - $I_\perp$, Solid Line - ΔV

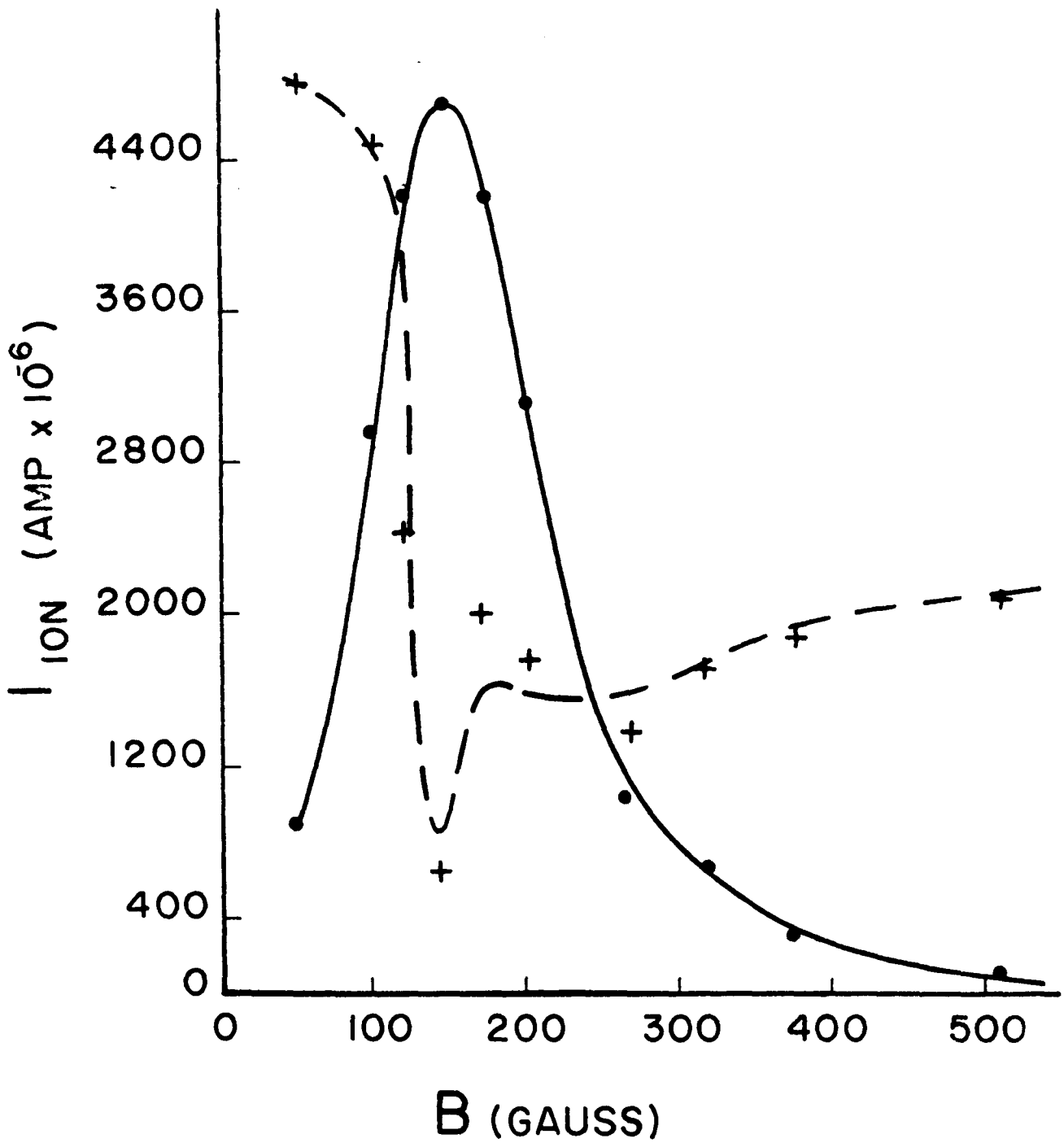

Fig. 3-13 Ion Currents at the Terminal Particle Collector vs. Magnetic Field

Solid Line - Inner Collector Current Broken Line- Outer Collector Current

particle collector. The variation of $D_\perp$ (inner collector) with field is similar to that obtained with the radial particle collector; i.e. the ratio of $D_\perp$ at 510G to that at 175G is 13.7 from inner terminal particle collector data and 8.5 from radial particle collector data. As with radial collector derived $D_\perp$, the diffusion coefficient drops as the cell-forming beam envelops the plasma column.

2) Effect of BN Electron Shield

Density and transverse flux data have been gathered for operation in which electrons from the bombarding filament are kept from entering the column by the imposition of a BN shield about the cathode (Fig.2-7). n_p and end plate current are shown in Fig.3-9. Note that these quantities are diminished by the shield compared to the shieldless data (Figs. 3-4 and 3-5), and that they fall with B; i.e., $n_p = 3.4 \times 10^{10}$ cm^{-3} at 1180G down to 0.048×10^{10} cm^{-3} at 100G. $D_\perp$, plotted with field in Fig.3-11, falls as B increases. From 200-850G, $D_\perp$ varies roughly as B^{-1}, suggestive of so-called Bohm diffusion[1] in this range. The regular variation of $D_\perp$ with field when the column is shielded against incursion of high energy electrons invites comparison with the $D_\perp$-B plot when electrons are free to enter the column (Fig.3-11). In the latter case, $D_\perp$ falls as cells set in and is minimal where cells are best developed, being nearly two orders of magnitude smaller than in the shielded column at 200G.

At fields below 500G, the potential well with the shield in place is not as steep as it is without the shield, and ΔV is lower as well. Er drops with B (Er = 760V/M at 715G, Er = 160V/M at 200G) as $D_\perp$ rises. Δ V drops off with B as well, from 1.2V at 850G to 0.4V at 50G.

3) Double-ended Operation

The Q-machine was operated double-ended to investigate the effect of surrounding a conventional plasma column with a tubular beam of energetic electrons, this beam being either cellular, possessing considerable transverse energy, or thin and having its energy in the longitudinal direction (impregnated cathode emitter).

a) Both ends electron shielded

Double ended operation with BN electron shields at both ends (one end generating plasma) results in raising ion density over that of single-ended operation. For example at 850G, $n_p = 2.0 \times 10^{10}$ cm^{-3} single-ended, $n_p = 3.0 \times 10^{10}$ cm^{-3} double-ended; at 265G, $n_p = 0.31 \times 10^{10}$ cm^{-3} single-ended, $n_p = 0.50 \times 10^{10}$ cm^{-3} double-ended. The depth of potential well tends to drop as the magnetic field is diminished in a manner exactly similar to the single-ended situation. $I_\perp$ falls as B increases, much as in the single-ended mode. The ratio of n_p for double and single-ended operation varies little with field, but

rather with cathode temperature.

b) Plasma generating end shielded

The BN electron shield was removed from the non-plasma generating side to allow cell-forming electrons to enter at magnetic field range 120 - 320G and interact with the plasma column. As with single-ended operation without the electron shield, the shape of the potential well changes from a round-bottomed shape above 320G to a steep-walled double-humped shape below 320G when the cellular electron beam envelops the plasma column, and returns to a broad round bottomed shape below 100G when the cells have disappeared. The depth of the potential well increases markedly as this occurs ($\triangle V$ = 2.8V at 320G and 3.5V at 120G). The ratio of n_p for double and single-ended operation increases sharply below the cellular onset field as a result. Values for n_p are 1.2×10^{10} cm^{-3} at 510G (no cells), 1.9×10^{10} cm^{-3} at 200G (cells) and 0.01×10^{10} cm^{-3} at 50G (no cells).

$I_\perp$ drops when the field is lowered to allow electrons to envelop the column and deepen the potential well. $I_\perp$ is minimal when the well is at its deepest. $I_\perp / n_p$ is greatly diminished with double-ended operation in this mode; this quantity peaks just as cellular onset begins, and is cut to about a third of its value at 145G, where the cells are well-developed. Potential well depth $\triangle V$ is similar to that for the single-ended case; the latter is plotted in Fig.3-12. The inverse

relationship of ΔV and $I_\perp/n_p$ is borne out by these data; where cells are best developed, $I_\perp$ and $I_\perp/n_p$ are minimal and ΔV is maximal.

Increase in ion density via additional neutral flux will cause ΔV to drop and $I_\perp$ to correspondingly rise as in single-ended operation.

c) Plasma generating and shielded-impregnated cathode emitter

The impregnated cathode emitter (II - A3a) was placed at the non-generating end opposite the plasma generating end with the electron shield in place. A thin tubular beam of electrons with 1-2 kV longitudinal energy surrounds the plasma column. This beam could be injected at any field, and data were taken at fields up to 2.85 kG. Potential wells of a peculiar annular shape are produced, having rather steep walls (Fig. 3-14). The well depth depends highly upon beam intensity. The magnitude of this depth is much greater than that obtained with any other configuration, a value of 69 1/2 V was once obtained at 2.4 kG. The well depth and the steepness of its walls (Er) depends highly upon beam intensity. Higher intensity leads to higher values of n_p. Ion density profiles (Fig. 3-14) show the ionic population being drawn into the beam, this effect being more pronounced as the emitter current is raised. Note that although the central ionic density is cut approximately to a third, the peak density is increased by an order of magnitude or more. At 850 G, for example, central ionic density was 2.9×10^{10} cm^{-3} without the beam and 0.9×10^{10} cm^{-3} with

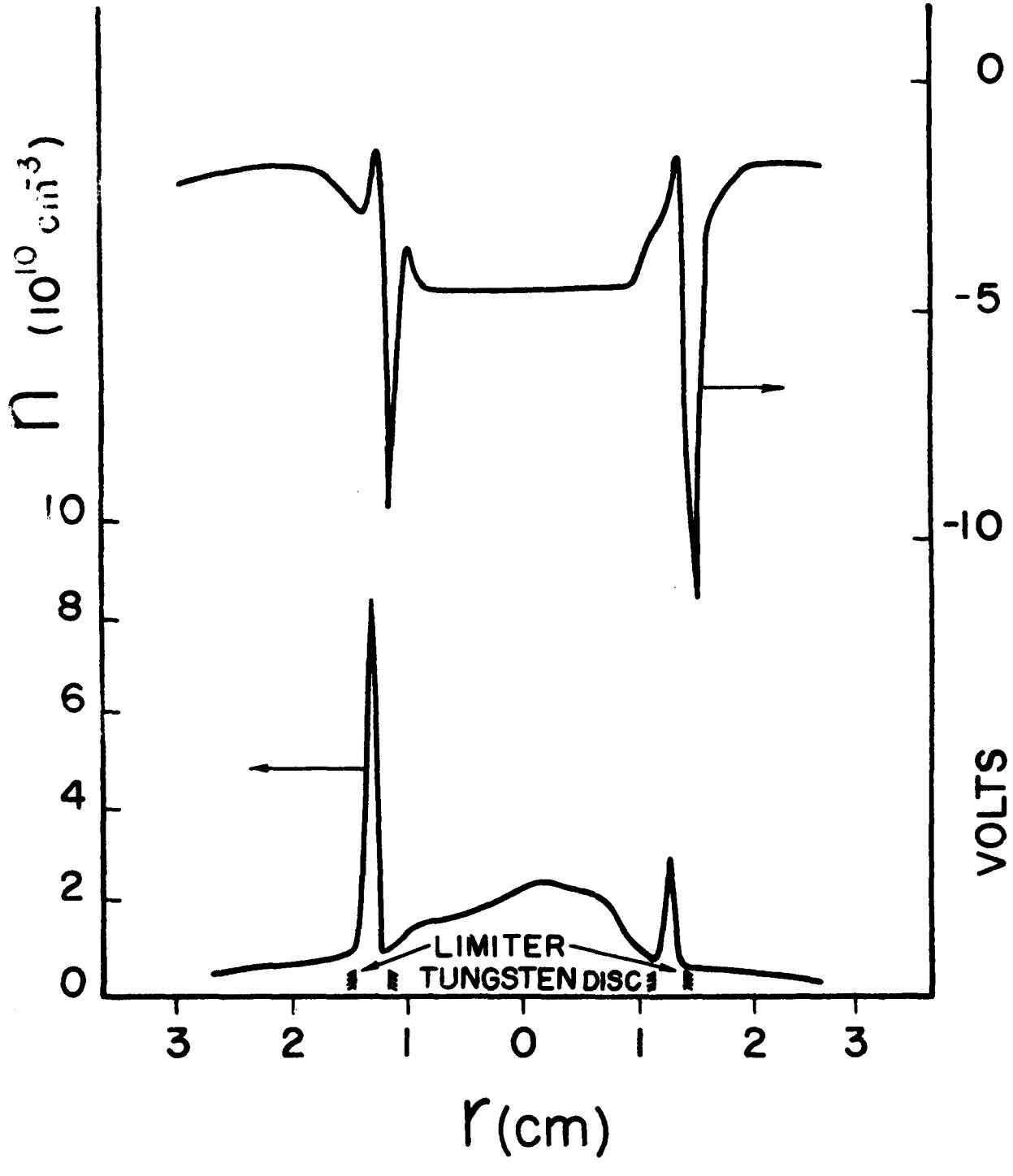

Fig. 3-14 Ion Density and Floating Potential Profiles at 2.4 kG with the Impregnated Cathode Emitter

the beam. Peak ion density in this beam is 65 x 10^{10} cm^{-3}. The ratio of n_p for single and double-ended operation in this mode is above 100 with the impregnated cathode emitter fully heated. With the impregnated cathode emitter at about 1410° K, $I_\perp$ was reduced by more than half, relative to single-ended operation at fields above 1.2 kG; $\triangle V$ was roughly doubled. n_p is about 3 to 6 times greater than with single-ended operation. $I_\perp / n_p$ is also reduced by the surrounding beam, that is, from 11 x 10^{-16} amp cm^3 to 0.2 x 10^{-16} amp cm^3 at 0.85 kG. The corresponding values of $\triangle V$ are 6.5 V and 18 1/3 V, demonstrating the plasma-confining efficacy of the deep potential well.

Most of the experimental data was taken with the impregnated cathode emitter running at 1410° K; the temperature of the tungsten hot plate adjacent to it was about 1650° K. The tungsten hot plate at the opposite plasma generating end was usually run at 2300° K.

Part C - Ancillary Experiments and Observations

1) Effect of Chamber Pressure

With an electron beam of up to 2.2 kV energy, the question of ionization of air is raised. Spectroscopic observation of the plasma column with an electron beam entering it revealed no characteristic spectral lines. At no time during the actual gathering of data for the entire set of experiments reported here was the column seen to glow.

The effect of background pressure upon ion density and columnar structure was investigated while operating single-ended in cell-generating configuration without the oven. Chamber pressures of 10^{-5} to 10^{-3} Torr were obtained by shutting off the diffusion pump. Ion density profiles and photographs show the column smearing somewhat at higher pressure. Cells were observed at all pressures. Ion density and collector current were, at most, four times as great at highest pressure as the lowest pressure; i.e. at 200G, $n_p = 7.0 \times 10^{10}$ cm^{-3} at 10^{-5} Torr and $n_p = 28 \times 10^{10}$ cm^{-3} at 0.9×10^{-3} Torr.

2) Cathode Sheath

Since many Q-machine phenomena depend on cathode sheath conditions, measurements were made to determine this condition under various configurations and operating conditions. If the cathode sheath be ion dominated, the ionizing capability of the cathode is saturated, and only an increase in cathode temperature will increase plasma density. If the cathode sheath be electron dominated, an increase in cathode temperature will increase density very little. Hence cathode sheath condition may be investigated by observing how ion density and collector current respond to rapid change in cathode temperature.

With the electron shield around it, the cathode was found to be ion dominated under all conditions. Without the shield, the cathode is ion dominated when no cells are produced.

When cells are generated, the cathode sheath is electron dominated under usual operating conditions. Ion domination was achieved while cells were observed by increasing the neutral flux. When this was done, oscillations were observed in all but the 100 - 320G range. The increase in atomic flux caused an increase in ion density, but n_p, $I_\perp$, and I (collector) varies with field in the same manner. Cellular size and columnar structure remained unchanged.

3) Temperature Measurements

The hot plate and limiter temperatures were measured with an optical pyrometer sighted through a transparent end cap. Temperatures were recorded at several places on the hot plate and limiter, with and without the electron shield in place, with and without outer filament current. Spacial variation in cathode temperature was found to be no more than about 30° K. In general, temperatures were those usually encountered in Q-machine operation. The temperature of the impregnated cathode emitter was measured over a range of power input. Spacial variation here was found to be less than 10° K. Temperatures ranged from 1360 to 1770° K.

4) Test for Secondary Emission

To determine the effect upon plasma current reading of secondary emission at current-collecting electrodes, the Q-machine was

operated single-ended with no neutral flux. The filament was biased 1.75 kV below ground, and the endplate collector biased to this value to reflect energetic electrons. The collector current was seen to vary with field in the same way as noted previously for the experimental runs (Fig.3-5) for which the endplate bias was much smaller (-200 to -300 V).

In a single-ended run without neutral flux, the impregnated cathode emitter ejected a 2 kV electron beam. There was initially sufficient ambient potassium in the chamber to yield an ion density profile on the order of 10^{10} cm^{-3}. After an hour, this potassium was nearly depleted; an ion density profile taken with quadrupled beam current yielded a density profile on the order of 0.2×10^{10} cm^{-3}. Were secondary emission from the probe a significant source of probe "current," this would not have been the case.

In a series of cell-generating experiments in which the neutral flux was progressively increased, the density profiles were seen to correspondingly rise; such would not have been the case if secondary emission dominated probe current.

Part D - Summary

Data and observations pertaining to cells in the C.C.N.Y, Q-machine and to the relationship of transverse diffusion to potential wells across the plasma column due to a peripheral electron beam has

been presented in this chapter.

Cell diameter was found to vary inversely with magnetic field and with the square root of filament-cathode potential.

The size of the cells and structure of the column was found to be invariant of neutral flux, cathode temperature, cathode sheath condition, current through the bombarding filament and length of column (30 - 0.6 cm). Blocking electrons emitted by the bombarding filament from the column eliminated cells and served to demonstrate that cells are caused by these electrons.

In single-ended mode, the onset of cells (emergence of high energy electrons) was accompanied by a deepening of a potential well across the column, intensification of inward-pointing radial electric field at the column edge, drop in transverse current and a large increase in ion density.

Injection of a thin electron beam of 2 kV longitudinal energy and relatively small transverse energy from an impregnated cathode emitter around a plasma column deepens the potential well across the column, reduces the ratio of transverse current to ion density, and increases peak ion density.

Injection around the plasma column of a cell-forming electron beam possessing considerable transverse energy also deepens the potential well across the column, reduces the ratio of transverse current to ion density and increases ion density, but the increase in

peak ion density is not as great as that due to the thin electron beam from the impregnated cathode emitter.

Over a hundredfold increase of pressure within the chamber increases ion density fourfold at most. Cathode sheath condition does not affect cellular structure. Observed plasma oscillations have not been found to correlate with transverse flux, ion density, or collector current.

Temperatures of the hot electrode assembly surfaces are those normally encountered in Q-machine operation; temperature changes have no qualitative effect on any of the phenomena reported here.

CHAPTER IV

THEORY AND CALCULATIONS

The experimental evidence presenter in chapter III shows, among other things, a negative correlation between the depth of the radial potential well across the plasma column and the perpendicular plasma current from that column. A calculation is made of the current of ions in the column that have the kinetic energy to surmount the well and be collected by the radial particle collector. From this, a mathematical relationship of ratio of $I_{\perp}/n_p$ for different potential well depths is obtained and compared with empirical data in this chapter.

Well depth difference is calculated using the von Goeler formula relating plasma potential and electron fluxes. This result is also compared with empirical data.

Since the entry of a high energy electron beam into the plasma column is accompanied by a large increase in ion density, an investigation is made as to the potassium ion current generated by collision of these electrons with neutral atoms and double ionization of singly ionized potassium.

Inquiry is made as to the nature of the instability that generates the oscillation in and about the electron beam created by the impregnated cathode emitter.

In order to test a hypothesis of the nature of the plasma cells described in the previous chapter, plots of equipotentials within the Q-machine electrode assembly are made and an electron trajectory calculated.

Part A - Calculation of Transverse Current

Measurements of $I_\perp$ (plasma current perpendicular to the magnetic field as gathered by the radial particle collector) and $I_\perp/n_p$ presented in the previous chapter along with measurements of the depth ΔV of the radial potential well across the column show $I_\perp$ and $I_\perp/n_p$ to correlate negatively with ΔV. This strongly suggests that the well serves to confine the ions, and with them, the electrons in the plasma.

To enable first order calculation of the confining effect of the well, a somewhat idealized model of the plasma is made. The plasma is assumed to be of average density n and to be situated at the bottom of the potential well. As is common in Q-machine work, the ions are assumed to have their transverse energy Maxwellianly distributed, with the temperature of the cathode. Since the equipartition time for thermalization of a 1-2 kV beam of

electrons with the plasma is many orders of magnitude greater than the transit time of a plasma particle, it may safely be assumed that the beam does not heat the plasma to any measureable extent. The ionic current collected by the radial particle collector is proportional to that fraction of particles in the plasma that have the kinetic energy to overcome the potential well.

The distribution of ions with kinetic energy w in the radial direction ($w = \frac{1}{2} m \dot{r}^2$) is[80]

$$dN_w = \frac{2N}{\sqrt{\pi}} (kT)^{-3/2} \sqrt{w}\, e^{-w/kT} dw \qquad (4\text{-}1)$$

where d Nw is the number of ions having kinetic energy between w and w+ dw, T the ion temperature, k is Boltzmann's constant, and N is the number of ions in the system. A kinetic energy of $q\Delta V$ is required to overcome the potential barrier ΔV(q = electronic charge). The current of these ions into an area a is

$$I_\perp = q a \int v_\perp dn_w = \frac{na}{(kT)^2} \sqrt{\frac{8kT}{\pi m}} \int_{q\Delta V}^{\infty} w\, e^{-w/kT} dw \qquad (4\text{-}2a)$$

or

$$\frac{I_\perp}{n} = q a \sqrt{\frac{8kT}{\pi m}} \left(1 + \frac{q\Delta V}{kT}\right) e^{-q\Delta V/kT} \qquad (4\text{-}2b)$$

The electrons are confined only by the ions in the column. They are assumed to diffuse outward to the radial particle collector at a rate proportional to the ion diffusion rate.

A meaningful comparison with experiment may be made by comparing ratios of $I_\perp/n$ obtained with different experimental runs with the potential wells. That is,

$$\frac{(I_\perp/n)_1}{(I_\perp/n)_2} = \sqrt{\frac{T_1}{T_2}} \left(\frac{1 + q\Delta V_1/kT_1}{1 + q\Delta V_2/kT_2}\right) e^{-\frac{q}{k}\left(\frac{\Delta V_1}{T_1} - \frac{\Delta V_2}{T_2}\right)} \qquad (4\text{-}3a)$$

For experiments run under identical cathode power inputs, $T_1 = T_2 =$ 2320° K. Then

$$\frac{(I_\perp/n)_1}{(I_\perp/n)_2} = \left(\frac{1 + q\Delta V_1/kT}{1 + q\Delta V_2/kT}\right) e^{-\frac{q}{kT}(\Delta V_1 - \Delta V_2)} \qquad (4\text{-}3b)$$

After taking the log of both sides

$$\ln\left(\frac{I_\perp}{n}\right)_1 - \ln\left(\frac{I_\perp}{n}\right)_2 = \ln\left(\frac{1 + q\Delta V_1/kT}{1 + q\Delta V_2/kT}\right) - \frac{q}{kT}(\Delta V_1 - \Delta V_2) \qquad (4\text{-}4a)$$

or

$$\frac{kT}{q}\left(\ln\left(\frac{I_\perp}{n}\right)_1 - \ln\left(\frac{I_\perp}{n}\right)_2\right) - \frac{kT}{q}\ln\left(\frac{1+q\Delta V_1/kT}{1+q\Delta V_2/kT}\right) = \Delta V_2 - \Delta V_1 \qquad (4\text{-}4b)$$

Since the electron current is assumed to be proportional to the ion current, the ratio of the collected currents $I_\perp$ should equal the ion current ratio. For a typical cathode temperature of 2320° K,

$$\frac{1}{5}\ln\left(\frac{I_\perp}{n}\right)_1 - \frac{1}{5}\ln\left(\frac{I_\perp}{n}\right)_2 - \frac{1}{5}\ln\frac{1+5\Delta V_1}{1+5\Delta V_2} = \Delta V_2 - \Delta V_1 \qquad (4\text{-}5)$$

where ΔV is in volts. The third term on the left side is relatively small.

Values of $I_\perp/n_p$ and ΔV were assembled for an experimental run with a column shielded from electron entry (1), and for a run in which the "cellular" electron beam entered the column (2). The left and right sides of eq.4-5 are plotted separately versus magnetic field in Fig.4-1. Agreement is seen to be good despite the simplifying assumptions made in the derivation of eq.4-5.

Part B - End Condition

In order to estimate the increase in radial potential well depth due to the formation of an ion sheath at the periphery of the cathode by electrons from the bombarding filament, it is assumed that the current of this beam incident on an annulus of the cathode of area A

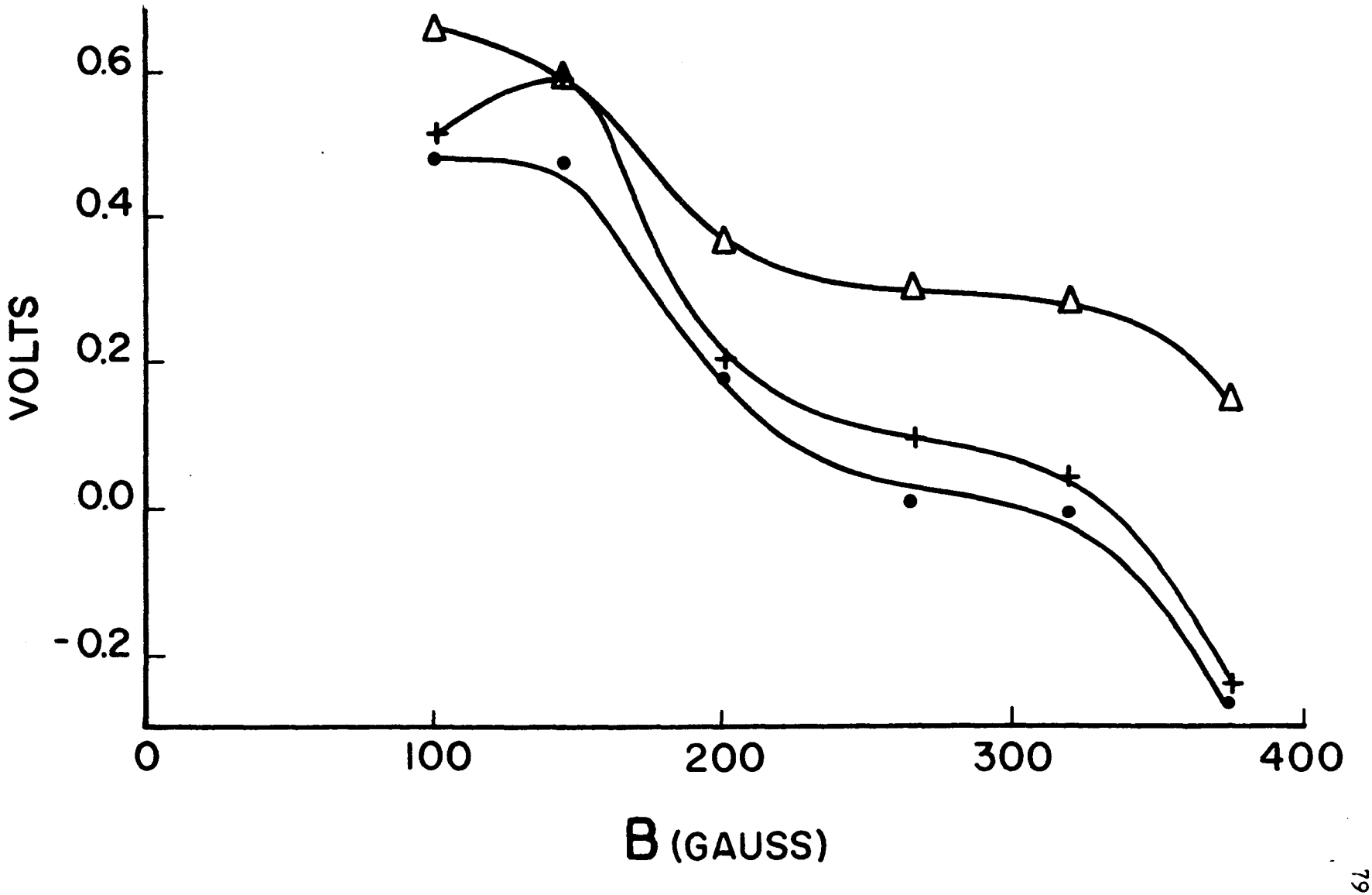

Fig. 4-1 $\Delta V_2 - \Delta V_1$, Measured and Calculated vs. Magnetic Field

\+ Empirical $\Delta V_2 - \Delta V_1$ • - Left Side of eq. 4-5 Δ - Right Side of eq. 4-9

is equal to the fast electron current I entering the column.

Without this current, the plasma potential ϕ_p is given by von Goeler, (eq.9b Ref.81):

$$\phi_p - \phi_w = \frac{kT}{q} \ln \frac{1/4 n_e \bar{v}^-}{R_i(T)} \tag{4-6}$$

where ϕ_w is the cathode potential ($\phi_w = 0$, since the cathode is grounded), n_e the electron density in the plasma, q = electronic charge, $\bar{v}^-$ is the mean speed of the plasma electrons. $R_i(T)$ is the Richardson-Dushman function for thermionic flux. This equation was obtained by equating the electronic flux into the cathode to that leaving the cathode (thermionic emission). If bombarding electrons strike the cathode, this flux must be added to the incident plasma flux:

$$\phi_p' = \frac{kT}{q} \ln \frac{1/4 n_e \bar{v}^- + j_b}{R_i(T)} \tag{4-7}$$

where $j_b = \frac{I}{qA}$ is this extra flux. The difference in plasma potential $\phi_p' - \phi_p$ for the two cases (electron shielded, case 1 and cell-generating, case 2), assuming equal temperatures is given by

$$\phi_{p_2} - \phi_{p_1} = \frac{kT}{q} \ln \left(\frac{n_{e_2}}{n_{e_1}} + \frac{j_b}{1/4 n_{e_1} \bar{v}_e^-} \right) \tag{4-8}$$

The difference in well depth for the two cases $\Delta V_2 - \Delta V_1$ is taken to be this plasma potential difference. For T = 2320°K we have

$$\Delta V_2 - \Delta V_1 = \frac{1}{5} \ln \left(\frac{n_{e_2}}{n_{e_1}} + \frac{J_b}{0.78 \times 10^5 n_{e_1}} \right) \text{VOLTS} \quad (4\text{-}9)$$

I was obtained by placing an endplate, biased to collect electrons, close to the limiter with no neutral flux incident on the cathode. The bombarding filament was heated to its operating value and was initially unbiased. The -2 KV bias was switched on, the collector current jumped to some value, then slowly rose as the cathode heated. This initial value is taken as I. The bombarded area A on the cathode is taken as an annulus at the outer rim of the plasma column, 2 mm thick.

Relevant data for the same experimental runs reported in Part A were assembled. $\Delta V_2 - \Delta V_1$ from eq. 4-9 is plotted vs B in Fig. 4-1.

Part C - Calculation of Collisional Ion Current

Since the entry of electrons of 1-2 K V energy into and around the plasma column is accompanied by a large increase in ion density and collector current, a question arises as to whether this increase may be attributed to ionization of neutral atoms or double ionization of potassium by the electron beam. For these calculations, a potassium ion density of 10^{11} cm^{-3} and a neutral atom density of 10^{10} cm^{-3} are assumed.

The cross-section for ionization by electron bombardment is given as[82]

$$\sigma = \frac{\bar{\mathcal{F}} a \ln(\mathcal{E}/\bar{x})}{\bar{x}\,\mathcal{E}} \quad cm^2 \qquad (4\text{-}10)$$

where $\mathcal{E}$ is the electron kinetic energy in eV, $\bar{x}$, the weighted mean ionization potential, $a = 4.0 \times 10^{-14}$ and $\bar{\mathcal{F}}$ is an empirical constant. For single ionization by collision $\bar{\mathcal{F}} = 5.7$, $\bar{x} = 10.4$, $\mathcal{E} = 2$ keV, and

$$\sigma = 5.77 \times 10^{-17} cm^2$$

The number of ions produced per cm of electron path is given by

$$n\sigma = 10^{10} \times 5.77 \times 10^{-17} = 5.77 \times 10^{-7} \frac{ions}{cm} \qquad (4\text{-}11)$$

If the electron path be very nearly straight, as is the case with the beam out of the impregnated cathode emitter, one merely need multiply this quantity by the column length (50 cm) to get the number of ions produced in the plasma column per electron. This number then, multiplied by the electron beam current, gives the ionic current produced in the column:

$$\frac{I_{ion}}{I_{elec.\,beam}} = 5.77 \times 10^{-7} \frac{ions}{cm} \times 50\,cm = 2.88 \times 10^{-5} \qquad (4\text{-}12a)$$

(beam from impregnated cathode emitter)

With a cellular beam, the path length is longer due to the helical path of the electron beam. At 200 Gauss, the path is 1.26

times the length of the column. Therefore

$$\frac{I_{K^+}}{I_{elec.\ beam}} = 3.83 \times 10^{-5} \text{ (cellular beam)} \quad (4\text{-}12b)$$

For second ionization of singly ionized potassium by electron collision, the relevant parameters are $\bar{S} = .217$, $\bar{x} = 34.2$, and hence $\sigma(K^+ \rightarrow K^{++}) = 1.77 \times 10^{-17}$ cm^2, and in 1 cm of path length the electron doubly ionizes

$$n\sigma = 10^{11} \frac{\text{ions}}{\text{cm}^3} \times 1.77 \times 10^{-17} \text{ cm}^2 = 1.77 \times 10^{-6} \frac{\text{ions}}{\text{cm}} \quad (4\text{-}13)$$

Therefore,

$$\frac{I_{K^{++}}}{I_{elec\ beam}} = \begin{cases} 8.85 \times 10^{-5} & \text{(impreg. cath. beam)} \\ 11.2 \times 10^{-5} & \text{(cellular beam)} \end{cases} \quad (4\text{-}14)$$

The electron beam current was investigated in the following way. An end plate, biased to collect electrons, was placed less than 1 cm from the limiter in the electrode assembly. The filament was heated to its normal operating temperature, but left unbiased. The -2 kV bias was switched on, and the instantaneous collector current was read. The collector current rose slowly after this quick jump from zero due to thermionic emission as the cathode slowly heated. The

initial value of the collector current is taken as the electron beam current that enters the column. With the impregnated cathode, the greatest observed beam current was found to be 1.2 ma. The sum of collisional singly and doubly ionized currents is 0.1^{6} μA (impregnated cathode beam). With the cell-forming beam, the greatest observed beam current was found to be 2.1 mA. The sum of collisional singly and doubly ionized currents is .31μA (cellular beam).

These currents are but a small fraction of the ionic current collected at the end plate (Fig. 3-5).

Part D - Oscillation in the Energetic Electron Beam

Under normal operating conditions, oscillation in the plasma is not observed when the cell-forming electron beam surrounds the plasma column. When the thin circular beam (from the impregnated cathode emitter) is injected into the experimental volume, either to engulf the plasma column or in the absence of the column, oscillations in the 23-340 kHz range of several mv amplitude are observed in the beam. The frequency is virtually invariant to magnetic field and neutral flux, but varies strongly with beam intensity. The cause of this oscillation shall be sought.

The instability of an electron beam moving parallel to a magnetic field due to slippage in its velocity profile is well-known in microwave devices[83,84]. Investigation of diocotron instability in

plasma is only quite recent[41,85].

Buneman, Levy, and Linson[84] define a stability parameter $q \equiv nm/\epsilon_0 B^2$. The beam is stable if $q < 0.1$. Substituting numbers for the electron mass m and ϵ_0, we have the stability criterion $n/B^2 < 10^{18}$, where n is electrons/meter^3 and B is in Teslas. A typical magnetic field used in these experiments is about 1 kG, and an upper limit to the electron density is $\sim 10^{14}$ M^{-3}. This gives $n/B^2 \simeq 10^{16}$. The beam is diocotron stable under this criterion. Stix[85] derives a diocotron stability criterion for the case of an electron beam bordered plasma (similar to the actual situation here): $\tanh kb < \frac{k^2 d^2 r^2}{4(1+r)}$ where b is the distance from the beam to the chamber wall, d the beam thickness and $r \equiv \frac{4\pi n_i M_i c^2}{B^2}$ (Gaussian units). $\vec{k}$ is in the transverse direction. With typical operating conditions: B = 1 kG, $n_i \cong 10^{10}$ cm^{-3}, substitution of the relevant numbers leads to the requirement that for instability, the wavelength $2\pi/k$ must be greater than 54 cm. Since the wavelength is in the transverse direction, this is clearly impossible for a beam diameter of about 2.6 cm.

Drift instabilities[2], be they resistive[11] or due to pressure, temperature or density gradients[12,13] have a term proprtional to $\frac{kT}{qB}$ in the dispersion relation (here k = Boltzmann constant, q = electronic charge). The dispersion relation for flute instability depends strongly on B. The dispersion relation for the Kelvin-Helmholtz instability[86] is dependent on B through terms inversely proportional to the Larmor

frequency; the cyclotron instability occurs at or near multiples of the Larmor frequency[2]. There is also a significant dependence of the dispersion relation on plasma density for density gradient drift, resistive drift, flute and Kelvin-Helmholtz instabilities. Since the frequency of the observed oscillation depends little on plasma density and is virtually unchanged as the magnetic field is varied over an order of magnitude while other parameters are unchanged, one may exclude drift, flute, Kelvin-Helmholtz, and cyclotron instabilities as the cause of oscillation in the beam.

The insensitivity of the oscillation to magnetic field and ion density, its dependence on beam intensity and its high frequency leaves an electrostatic wave as the most likely candidate. Perhaps this wave is excited by a two-stream instability of the beam and its background.

Part E - Electron Trajectory Calculation

In order to calculate the trajectory of an electron leaving the bombarding filament, the electric field within the assembly must be known. For this purpose, plots of equipotentials within the assembly were obtained using a potential plotting device. Electron trajectories were calculated in intervals between equipotentials using the Lorentz force law.

Models of diametric axial cross-sections of various configurations of the assembly were made by fastening strips of aluminum

foil corresponding to electrodes onto teledeltos paper with silver conducting paint. The models are to 4:1 scale. The various electrode assembly configurations that were modelled and plotted are as follows:

i - cell-yielding configuration - all shields - 3/4 inch limiter aperture

ii - cell-yielding configuration - all shields - 1 inch limiter aperture

iii - cell-yielding configuration - all shields - $\frac{1}{2}$ inch limiter aperture

iv - cell-yielding configuration - all shields - no limiter

v - cell-yielding configuration - no inner shield - 3/4 inch limiter aperture

vi - cell-yielding configuration - no cathode - 3/4 inch limiter aperture

Although the equipotentials were plotted for a two-dimensional projection of the assembly, the electrons stay sufficiently close to the surfaces to assure small deviation from the true three-dimensional equipotentials in an azimuthally symmetric arrangement. An equipotential plot with the model of the assembly with 3/4 inch limiter aperture is shown in Fig. 4-2. To make calculation possible, space charge effects are neglected. The trajectory of an electron leaving the filament with zero initial speed ($qV \gg kT$) is calculated in the following way. A line from the point of emission to the nearest equipotential, perpendicular to this equipotential, is drawn. Transverse and longitudinal components of this line are measured. The transverse and longitudinal velocities $v_\perp$ and v_{11} are computed, such that $v_\perp^2 = v^2 \sin^2\theta$ and $v_{11}^2 = v^2 \cos^2\theta$, where θ is the

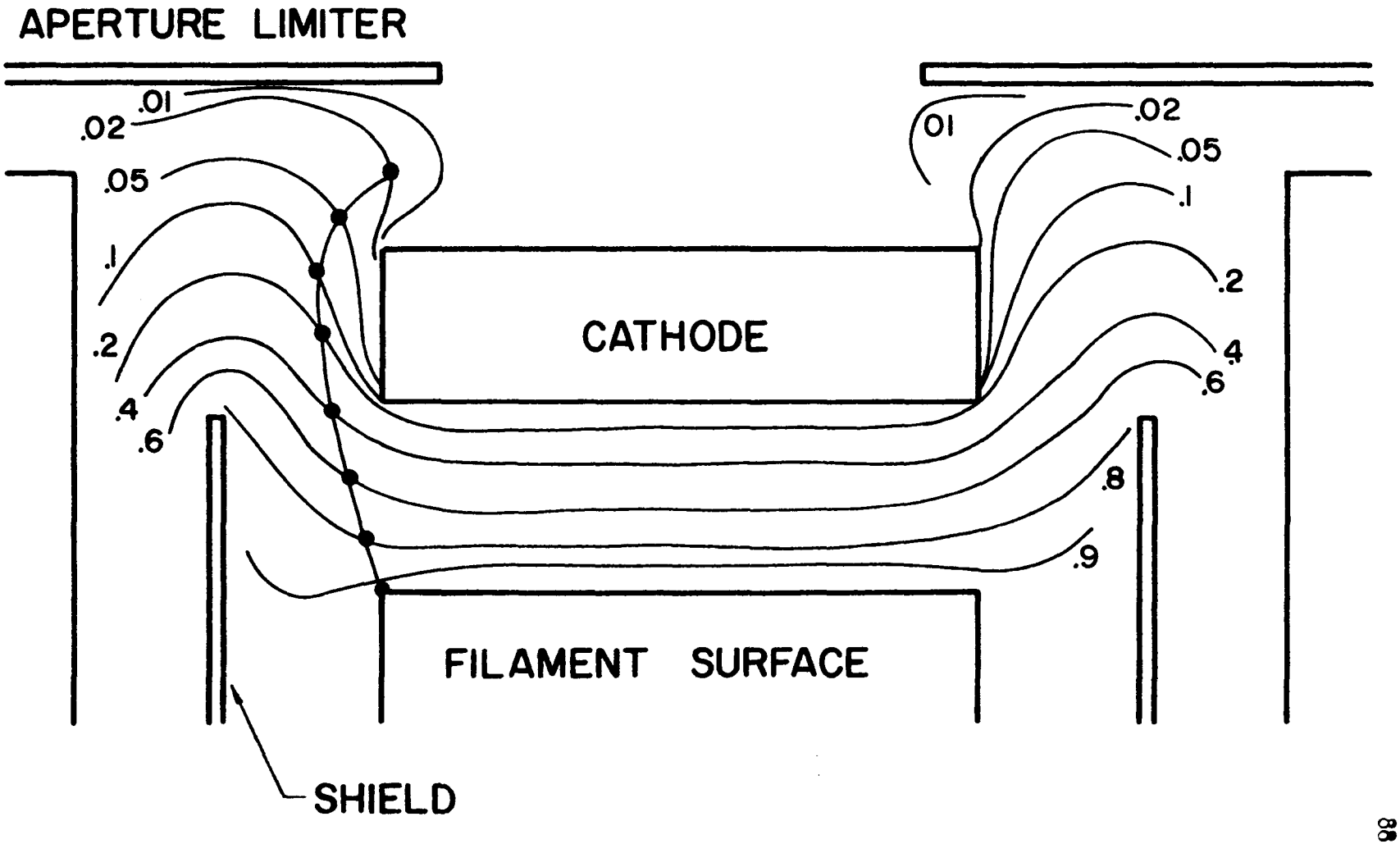

Fig. 4-2 Model of Cell-generating Electrode Assembly with Equipotentials and Electron Trajectory

initial pitch angle and $v^2 = \frac{2\,e\,V}{M_e}$, being the potential drop in this interval. The Larmor frequency $\omega = eB/M_e$ is computed, as well as the "final" Larmor radius $r = v_\perp/\omega$. The longitudinal distance travelled by the electron making a complete rotation with this Larmor frequency if the electron encountered no further longitudinal acceleration is $z \equiv v_{11}\, 2\pi/\omega$. The actual longitudinal component of the distance between the point of emission and the nearest equipotential x is measured. The phase angle of Larmor rotation at this equipotential, $\phi \equiv x/z$ is found. (In all computations done here, $x < z$). The guiding center of the electron is taken to follow the line from the point of emission to the nearest equipotential. The electron is radially displaced a distance $r \sin\phi$ from the point of intersection of the guiding center and this equipotential; this is the new starting point. A line from this point to the next equipotential line, perpendicular to the latter is drawn. The additional $v_\perp$ and v_{11} gained by the electron going between these equipotentials are found and added to the previous value. The radial displacement from the guiding center intersection $r' \sin\phi'$ is obtained, and a line drawn from there to the next equipotential, etc., until the electron strikes a surface or approaches the limiter aperture to enter the plasma column.

It was found that an electron emitted from the outer periphery of the filament, with V = 2 kV and B = 200 G, approaches the limiter aperture with a final Larmor radius of 4.95 mm. Photographs show cells of $4\frac{1}{2}$ mm radius under these conditions, matching the calculated radius with 10% deviation.

Part F - Summary

Calculation of the confining effect of a radial potential well in the column, and comparison with experimental data has been done. An idealized model of the plasma was made and the current of ions in the tail of the radial energy distribution that have the kinetic energy to surmount the potential well was computed. This current sharply falls with increasing well depth $\triangle V$. A relationship of ratios of L/n to potential well depths has been derived. Comparison with empirical data (Fig.4-1) is surprisingly good in view of the simple model and assumptions made in this derivation.

The difference in well depths obtained with and without the cell-forming beam was calculated according to the von Goeler formula and compared with the empirical difference.

The ionic current generated by ionization of neutral potassium in the chamber by the energetic electron beam and the additional current due to double ionization of potassium has been calculated and found to be a very small fraction of the collected ion current.

Inquiry was made into the cause of observed oscillation in and around the electron beam emanating from the impregnated cathode emitter. Diocotron, drift, flute, Kelvin-Helmholtz and cyclotron instabilities were excluded as the generator of oscillation. It seems most likely that an electrostatic wave was observed.

Equipotential plots for models of the Q-machine electrode assembly were traced and a trajectory calculation made for an electron leaving the edge of the bombarding filament. It was found that the electron could enter the column at a field for which cells were observed; its Larmor radius differs from the cell radius by but 10%.

CHAPTER V

DISCUSSION AND CONCLUSION

This chapter includes a discussion of the more important experimental results, a comparison of these with the theory presented in Chapter IV and some concluding remarks.

The most significant experimental findings - relationship between a radial potential well and transverse diffusion - are summarized in part A.

The mechanism whereby the energetic electron beam deepens the potential well is discussed in part B.

A review of the theory relating perpendicular diffusion and potential well depth is presented in part C. This section includes an attempt to explain the density profiles presented in chapter III.

A review of the cellular observations, phenomena, and cause comprises part D.

Part E forms the conclusion of this work and includes a discussion of a possible extension of the mechanism.

Part A - Summary of Experiment

With the Q-machine in single-ended mode and the electrode assembly shown in Fig. 2-3, the radial density profile above 500G

appears somewhat Gaussian and the floating potential profile shows a flat-bottomed potential well (Fig.3-2). As the field is lowered below about 320G (with circular limiter of 3/4 inch diameter), electrons from the bombarding filament enter the column around the cathode, producing a cellular pattern about the column. The depth of the potential well increases at the column edge (Fig.3-6). Density and end plate collector current increase sharply as the transverse current, the ratio of transverse current to peak ion density, and the perpendicular diffusion coefficient all drop (Figs.3-4, 3-10). These quantities reach an extremum at about 140 - 200G. Transverse diffusion varies inversely with potential well depth, as does cell radius with magnetic field. The cell radius varies as the square root of the filament-cathode potential.

These phenomena are qualitatively unchanged with variation of limiter diameter, bias or material, variation of column length, electrode temperature, degree or absence of neutral flux.

With an impregnated cathode emitter projecting a beam enveloping the plasma column generated at the opposite end (with electron-blocking BN shield in place), ion density is increased over that obtained without the beam. A deep gorge of a potential well is created (Fig.3-14) cutting transverse diffusion. Since an electron beam is emitted at all magnetic fields, this is the case for all fields.

Part B - Cause of Potential Well

It was seen that the emergence of a fast beam of electrons with a Larmor radius of several millimeters or near zero entering into and/or around the plasma column is accompanied by a peaking of the potential profile in the vicinity of the beam and increase in potential well depth. The question arises as to how this beam accomplishes this increase.

The thin beam from the impregnated cathode emitter is about 1.6 mm thick. From the known beam current, area and speed, it is calculated that the electron density is at most on the order of 10^8 electrons cm^{-3}.

The potential drop across the beam in vacuo is calculated to be about 1/3 volt; since the plasma density in the vicinity of the beam (with no beam in that region) is at least comparable to this beam density, one would expect the conductive and dielectric effects of the plasma to suppress the space charge influence of the beam. Actual well depths are greater than 1/3 volt, even without the beam; with the beam, the depth was found to be at times in excess of 6 volts.

The causes of the well depth increase may be attributed to end conditions. It is well known that the latter can establish the radial density and potential profiles in a Q-machine[22,86-90]. It has been reported in chapter III that emergence of a cell-forming peripheral electron-beam is accompanied by a change in cathode sheath condition from ion to electron dominance. There is a preponderance of electrons

especially at the outer region of the cathode; secondary emission of electrons from the bombarded undersurface of the limiter may also contribute to this preponderance. The same would be the case with the impregnated cathode emitter.

A series of experiments provides some supporting evidence for this conjecture. With a cell-forming electron beam around the column and an electron-rich cathode sheath, the neutral flux was increased to force a change in sheath condition to ion dominance. The potential well was seen to become broader and shallower as this change took place.

The near-agreement of the calculated difference in well depths (IV-B) also suggests that end conditions are the dominating effect here. It also implies that there is no substantial source of plasma outside the cathode, be it from collisional ionization or phantom "density" from secondary emission from current-collecting electrodes.

Part C - Potential Well and Ion Confinement

An important experimental finding reported in chapter III is that the onset of electron beam emergence into the plasma column is accompanied by increase in potential well depth and subsequent increase in peak ion density in the column and in longitudinal flux as well as a decrease in transverse flux. A relation between the current of ions in the column that could energetically surmount the potential well of depth ΔV has been derived in section IV-A: $I_\perp \propto n\left(1+\frac{q\Delta V}{kT}\right)e^{-\frac{q\Delta V}{kT}}$

Ratios of L/n for two well depths enable comparison of empirical data with this relation through cancellation of factors. The result, plotted for an instance in Fig.4-1, appears to verify the theory, derived with the aid of idealizations and assumptions.

It is concluded here that the potential well serves to confine ions by creating a radial barrier to all but the more energetic ions in the ionic radial kinetic energy distribution; the greater the depth of the well, the fewer the number of ions can surmount it. As ions diffuse outward from the core of the plasma column, they are repelled by this radial electric field. The electric field also alters the trajectory of the ions so that in their motion they spend relatively more time at the portion of their path nearest the well bottom. It may be said that this is a form of ion trapping. Since the well bottom is radially at the same position as the electron beam, the ion density is peaked at this position; that is the case for the cellular beam (Fig.3-6) or for the thin beam (Fig.3-14). Where the width of the potential well is smaller than the ion Larmor radius, this electrostatic confinement dominates over the magnetic confinement.

Part D - Cellular Etiology

Several empirical facts indicate that electrons streaming around the bombarding filament generate the plasma cells shown in Fig.3-3.

1) Imposition of a shield blocking entry of electrons completely elimin-

ates cells.

2) The cell radius varies inversely with the magnetic field and as the square root of the filament-cathode potential.
3) Imposition of limiter bias equal to the filament-cathode potential eliminates cells.
4) Cells are observed in the near absence of a plasma column.

Calculation of electron trajectory under conditions in which cells were observed shows that electrons from the periphery of the bombarding filament may enter the column, and that the Larmor radius is approximately equal to the cell radii photographed under the same conditions. Placement of an outer filament biased to the same potential as the bombarding filament results in the creation of cells at a higher field. The existence and radius of the cells is a function of magnetic field, filament-cathode potential, and electrode geometry exclusively. Although it is not known why the electron beam assumes a pattern of discrete cells, the above evidence is conclusive on the question of their origin. Given a uniform magnetic field, a vacuum chamber and power supplies, cells can be created via construction of a suitable electrode configuration.

A hypothesis, recently proposed, that the cells are a hydromagnetic analog of convective Taylor cells[63,64] has been found to be untenable.

Part E - Summary and Conclusion

The central feature of the experimental investigation reported here is the depression of a radial potential well across the plasma column by a peripheral beam of fast electrons and the subsequent increase in ion density and cut in transverse flux. Where the beam was present, this was the case at all magnetic fields and beam energies.

A relation between well depth and fraction of ions that surmount it was derived and a comparison with empirical data was made; agreement was found to be quite good. The ions can be said to be electrostatically confined; increase in well depth decreases transverse flux and increases ion density and longitudinal current.

The structure and magnitude of the potential well is attributed to end condition. The cell-forming beam was seen to create an electron-rich sheath at the hot plate and may well create an electron sheath about the limiter rim in that region; this would tend to depress the potential of the plasma where magnetic field lines are tied to the sheath. The ion spends more of its time, relatively speaking, in the region of lower potential, resulting in a peak of ion density at the well bottom; in this way ions are effectively trapped there. The shape of the density profile is thereby dictated in large part by the potential profile.

Stix has proposed a device for confinement of ions by a potential well across a plasma column[91,92]. From the evidence presented here, it is seen that such a device has been simulated in a Q-machine. This

principle may be extended to other devices by appropriate adjustment of end conditions and/or enveloping a plasma column in a sufficiently dense tubular beam of energetic electrons.

From all evidence presented in the previous section of this chapter, it is seen that the phenomenon of cells observed here is due to a combination of electrode assembly geometry, bias, and magnetic field; the cells per se do not appear to affect plasma confinement.

REFERENCES

1 D. Bohm, E.H.S. Burhop and H.S.W. Massey, in The Characteristics of Electrical Discharges in Magnetic Fields, A. Guthrie and R.K. Wakerling, Eds. (McGraw-Hill, New York 1949).

2 B.B. Kadomtsev, Plasma Turbulence (Academic Press, New York 1965).

3 N. D'Angelo and N. Rynn, Phys.Fluids 4, 275 (1961).

4 N. D'Angelo and N. Rynn, Phys.Fluids 4, 1303 (1961).

5 N. D'Angelo, Phys.Fluids 7, 1086 (1964).

6 S. von Goeler, Phys.Fluids 8, 1570 (1965).

7 N.S. Buchel'nikova, A.M. Kudryavtsev and R.A. Salimov, Soviet Physics-Technical Physics 10, 53 (1965).

8 N.S. Buchel'nikova, Nucl. Fusion 6, 122 (1966).

9 N.S. Buchel'nikova, R.A. Salimov, and Yu.I. Eidelman, J.E.T.P. 25, 252 (1967).

10 N.S. Buchel'nikova, R.A. Salimov, and Yu.I. Eidelman, J.E.T.P. 25, 548 (1967).

11 F.F. Chen, Phys. Fluids 8, 912 (1965).

12 H.W. Hendel, T.K. Chu, and P.Politzer, Phys.Fluids 11, 2426 (1968).

13 T.K. Chu, H.W. Hendel, and P. Politzer, Phys.Rev. Lett. 19, 1110 (1967).

14 N. Wolf and K.C. Rogers, Phys. Fluids 9, 2294 (1966).

15 K.C. Rogers and N. Wolf, Proc. 7th Conf. on Phenomena in Ionized Gasses, Belgrade Vol.II, p.137.

16 B. Eastlund, Phys. Fluids 9, 594 (1966).

17 B. Eastlund and K. Josephy, Phys.Fluids 9, 2400 (1966).

18 K. Josephy, B. Eastlund and T.C. Marshall, Phys.Fluids 10, 1112 (1967).

19 F.F. Chen, Phys. Fluids 9, 2534 (1966).

20 J.A. Decker, P.J. Freyheit, W.D. McBee, and L.T. Shepard, Phys. Fluids 10, 2442 (1967).

21 T.C. Simonen, T.K. Chu, and H.W. Hendel, Phys. Rev. Lett. 23, 568 (1969).

22 D.L. Jassby and R.W. Motley, Phys.Fluids 12, 258 (1969).

23 E. Guilino, Phys. Fluids 13, 1859 (1970).

24 D. Mosher and F.F. Chen, Phys.Fluids 13, 1328 (1970).

25 K.C. Rogers and F.F. Chen, Phys.Fluids 13, 513 (1970).

26 F.F. Chen, D. Mosher, and K.C. Rogers, Phys.Fluids 11, 811 (1968).

27 F.F. Chen, D. Mosher and K.C. Rogers, Phys.Rev.Lett. 18, 639 (1967).

28 G.S. Janes, R.H. Levy, H.A. Bethe, and B.T. Feld, Phys.Rev. 145, 925 (1966).

29 J.D. Daugherty, L. Grodzins, G.S. Janes and R.H. Levy, Phys.Rev. Lett. 20, 369 (1968).

30 S.V. Yadavalli, J. Electronics and Control 10, 429 (1961).

31 E. Canobbio, Nuovo Cimento 23, 1073 (1962).

32 J. Neufeld and H. Wright, Phys.Rev. 131, 1395 (1963).

33 W.T. Kennedy and K.G. Emeleus, Phys.Lett. 20, 165 (1966).

34 P.I. Blinov and L.P. Zakatov, Atomnaya Energiya 19, 233 (1965).

35 F.W. Crawford, Internat. J. Electronics 19, 217 (1965).

36 R. Leven, Beitr. Plasma Physik 6, 9 (1966).

37 P. Mills and H. Doucet, C.R. Acad. Sci. 266, 149 (1968).

38 M. Seidl and P. Sunka, Czech J. Phys. 18B, 289 (1968).

39 T. Idehara, Mem.Fac. Sci. Kyoto Univ. Ser. Phys. Astrophys. Chem. 32, 13 (1968).

40 R.J. Isaac, Canad. J. Phys. 47, 249 (1969).

41 R.H. Levy, J.D. Daugherty and O. Buneman, Phys.Fluids 12 2616 (1969).

42 V.J. Astrelin, N.S. Buchel'nikova, and A.M. Kudryavtsev Zh. Teck. Fiz. 40, 1185 (1970).

43 L.M. Field, K. Spangenberg, and R.Helm, Electrical Comm. 24, 108 (1947).

44 E.L. Gizton and B.H. Wadia, Proc.I.R.E. 42, 1548 (1954).

45 M.E. Hines, G.W. Hoffman, and J.A. Saloom, Jour. Appl. Phys. 26, 1157 (1955).

46 T.S. Lundgren and C.C. Chang, Phys.Fluids 5, 807 (1962).

47 W.H. Bostick, Phys.Rev. 104, 292 (1956).

48 W.H. Bostick, Phys.Rev. 106, 404 (1957).

49 D.R. Wells, Phys.Fluids 5, 1016 (1962).

50 W.H. Bostick and D.R. Wells, Phys.Fluids 6, 1325 (1963).

51 D.R.Wells and G. Schmidt, Phys.Fluids 6, 418 (1963).

52 W.H. Bostick, W. Prior and E. Farber, Phys.Fluids 8, 745 (1965)

53 D.R. Wells, Phys. Fluids 7, 826 (1964).

54 W.H. Bostick, W. Prior, L. Grunberger, and G. Emert, Phys. Fluids 9, 2078 (1966).

55 W.H. Bostick, Phys. Fluids 5, 1400 (1962).

56 D.R. Wells, Phys. Fluids 9, 1010 (1966).

57 R.W. Dory, D.W. Kerst, D.M. Meade, W.E. Wilson and C.W. Erickson, Phys.Fluids 9, 997 (1966).

58 W.L. Harries, S. Yoshikawa, and R.W. Palladino, Phys.Fluids 12, 1115 (1964).

59 W.L. Harries, Phys. Fluids 13, 140 (1970).

60 W.L. Harries, Phys.Fluids 13, 175 (1970).

61 G.O. Barney and J.C. Sprott, Phys.Fluids 12, 707 (1969).

62 F.F. Chen, D.Mosher, and K.C. Rogers, Proc. 3rd Int. Conf. Plasma Phys. and Controlled Nucl. Fusion Res. Vol.1, p.625 (Novosibirsk 1969).

63 J.C. Cataldo, Phys. Fluids 8, 2195 (1970).

64 J.C. Cataldo, Phys. Fluids 8, 2508 (1970).

65 R.L. Khyl and H.F. Webster, I.R.E. Trans. on Electron Devices, ED-3, 172 (1956).

66 H.F. Webster, Jour. Appl. Phys. 26, 1386 (1955).

67 H.F. Webster, Jour. Appl. Phys. 28, 1388 (1957).

68 C.C. Cutler, Jour. Appl. Phys. 27, 1028 (1956).

69 J.R. Pierce, I.R.E. Trans. on Electron Devices, ED-3, 183 (1956).

70 G.I. Kent, N.C. Jen and F.F. Chen, Phys.Fluids 12, 2140 (1969).

71 N. Rynn and N. D'Angelo, Rev.Sci. Instr. 31, 1326 (1960).

72 K.C. Rogers, G.E. Courville and N.S. Wolf, in Proceedings of the Conference on Physics of Quiescent Plasmas (Associazione Euratom - C. N.E.N., Rome 1967, Pt.1, p.259)

73 F.F. Chen, C.Etievant, and D. Mosher, Phys.Fluids 11, 811 (1968).

74 F.H. Coensgen, W.F. Cummins, W.E. Nexsen Jr., and A.E. Sherman, Rev.Sci. Instr. 35, 1072 (1964).

75 K.D. Sinel'kov, B.G. Safranov, V.G. Padalka, and I.I. Dimidenko, Zh. Tekh. Fiz, 33, 786 (1963).

76 J.C. Cataldo and C. Tao, Rev. Sci. Instr. (to be published).

77 F.F. Chen, in Plasma Diagnostic Techniques Chapt.4, R.H. Huddlestone and S.L. Leonard, Eds. (Academic Press, New York 1965).

78 F.W. Sears, Thermodynamics Chapt.11 (Addison-Wesley, Reading, Mass. 1953).

79 K.R. Spangenberg, Vacuum Tubes Chapt.4 (McGraw-Hill New York 1948).

80 F.W. Sears, Thermodynamics, op.cit., Chapt. 12.

81 S. von Goeler , Phys. Fluids 7, 463 (1964).

82 W. Lotz, Astrophys.Journal Suppl. 14, No.128, p.128 (1967).

83 E. Okress, Ed. Crossed-Field Microwave Devices (Acad.Press, New York 1961).

84 O. Buneman, R.H. Levy, and L.M. Linson, Jour. Appl. Phys. 37, 3203 (1966).

85 T.H. Stix, Phys. Fluids 14, 702 (1971).

86 F.W. Perkins and D.L. Jassby, Phys. Fluids 14, 102 (1971).

87 L. Enriques, A.M. Levine, and G.B. Righetti, Plasma Phys. 10, 641 (1968).

88 L. Enriques, A.M. Levine, and G.B. Righetti, Proc. 3rd Int.Conf. Plasma Phys. and Controlled Nucl. Fusion Res., vol.1, p.641 (Novosibirsk 1969).

89 C.W. Hartman and R.H. Munger, Proc. Conf. Quiescent Plasmas, Part 1, p.49 (Frascati 1969).

90 J.C. Cataldo, Plasma Phys. (to be published).

91 T.H. Stix, Phys. Rev. Lett. 23, 1093 (1969).

92 T.H. Stix, Phys. Fluids 14, 692 (1971).